



Supplement of

Source apportionment resolved by time of day for improved deconvolution of primary source contributions to air pollution

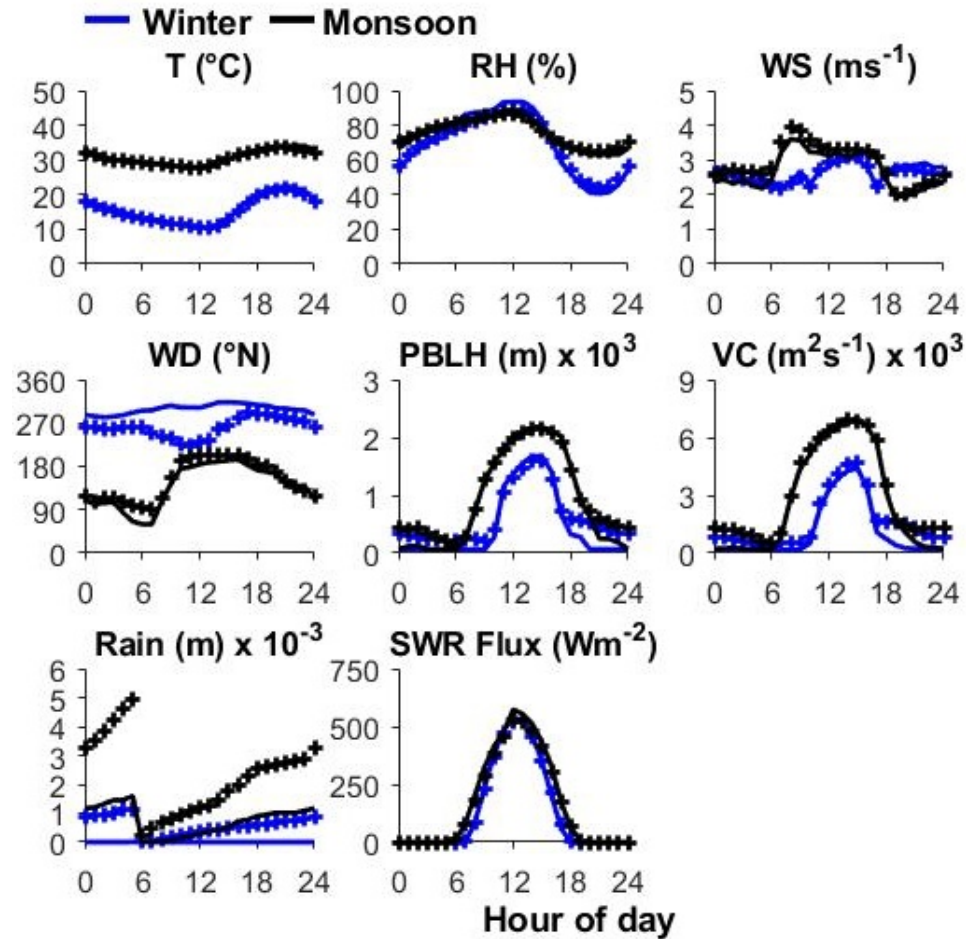
Sahil Bhandari et al.

Correspondence to: Lea Hildebrandt Ruiz (lhr@che.utexas.edu) and Joshua S. Apte (apte@berkeley.edu)

The copyright of individual parts of the supplement might differ from the article licence.

Additional Information for Proof of Concept for the Time-of-day PMF Approach

Note: To refer to PMF runs corresponding to specific time windows in the Supplement, we use the nomenclature “Season” + “Year” + “Period” in the format “SYTTTT”. For example, W171115 corresponds to the 1100–1500 LT of Winter 2017.



5

Figure S1 Diurnal profiles of meteorological parameters (temperature, relative humidity, wind speed, wind direction, PBLH, VC, rain, and SWR flux) by season. Mean (+) and median (—) values by season and hour of the day are presented. We retrieved visibility and relative humidity (RH) data from the Indira Gandhi International Airport (IGIA). To obtain mesoscale data for hourly wind speed, direction, temperature (10m above ground level), SWR flux, and planetary boundary layer height (H), we used the NASA meteorological reanalysis dataset (MERRA2). Precipitation data for Delhi was retrieved from the European Centre for Medium-Range Weather Forecasts' reanalysis dataset, ERA-Interim (Gani et al., 2019). The ERA-Interim 12-hour long assimilation windows for precipitation data are from 0600-1800 LT and 1800-0600 LT. The discontinuities in precipitation data occur where windows change. Similar discontinuities have been reported elsewhere as well (ResearchGate, 2021).

10

Table S1 Seasonal summary of PM₁ species—arithmetic mean (AM) for hourly concentrations.

	Winter	Monsoon
Org	112	23
NH ₄	20	4.6
Chl	23	0.4
NO ₃	24	3.6
SO ₄	16	10
BC	15	11
NR-	195	41

Table S2 Seasonally averaged meteorological variables in monsoon and winter 2017 (day-D/night-N)

Season	T (K) (D/N)	RH (%) (D/N)	VC (m ² /s)	PBLH (m) (D/N)	WS (m/s) (D/N)	WD (°N) (D/N)
W17	290/28 6	60/78	707/188	920/340	2.7/2.6	300/300
M17	305/30 2	71/81	3870/379 0	1600/460	3.4/2.5	250/190

S1 Steps for conducting PMF, criteria for factor selection, and R code

20 The first step to conducting PMF is the identification of strong, weak, and bad variables. Traditionally, average signal-to-noise ratio (SNR) is used as criteria for down-weighting species (Paatero and Hopke, 2003). However, selections based only on SNR are subjective and do not account for the ability of the model to fit the data. For example, data with SNR 1 may fit better than the data with SNR of 2. Here, we utilized data trimming prior to running PMF to account for the down-weighting of noisy or weak variables. We hypothesize that application of PMF will extract fewer than 8–9 factors. This is not surprising: most

25 AMS/ACSM studies report fewer than four factors (Jimenez et al., 2009). Even recent studies utilizing constraints report not more than 6 factors (Fröhlich et al., 2015; Canonaco et al., 2020). Thus, as pilot runs, we went to 9 factor solutions. In these pilot runs, a high Q/Q_{exp} can arise from few data points in the dataset ($Q/Q_{exp} > 50$ but going as high as O (1000)), biasing the overall Q/Q_{exp} . These time series points led to very high Q/Q_{exp} for specific m/z s as well. A representative figure from the PMF analysis of winter 2017 is shown in Fig. S2a–S Thus, we removed time points with $Q/Q_{exp} > 20$.

30 Our results suggested that removing these time series points prior to reweighting m/z s led to a dramatic reduction in the Q/Q_{exp} corresponding to the m/z s and therefore the number of m/z s that need to be down-weighted. Representative results for a single pass of data trimming at this decision step are shown in Fig. S3a–S In total, less than 15% of the data was removed before conducting PMF analysis for factor identification. Such data trimming is also considered standard procedure in PMF

analysis on data collected and analyzed at federal and state monitoring agencies (Dave Sullivan, *personal communication*).

35 Interestingly, the removed time series points were not necessarily associated with high concentrations. Histogram analysis suggests that while time series points with organic concentrations greater than $180 \mu\text{g m}^{-3}$ account for $\sim 10\%$ of the raw data, they account for $\sim 1\%$ of the removed points. Thus, the time series points at which PMF fails to fit appropriately are not necessarily associated with high concentrations. After removing data points that could not be fit by the PMF analysis even at 8–9 factor solutions, we utilized two criteria to identify “strong” and “weak” m/z s. The criteria used in the order of decreasing
40 importance were Q/Q_{exp} at an m/z (<10 for strong m/z) and, the slope and the correlation of modeled versus measured mass for contributions at an m/z (slope, $R > 0.7$). SNR of 1 was used as a check. The use of SNR of 1 is in line with the traditional definition since EPA PMF defines signal as data above noise (Norris et al., 2014). Only one m/z , m/z 12, was selected as a “bad” variable due to negative signals; this has been observed elsewhere as well (Fröhlich et al., 2015; Schlag et al., 2016). A full list of weak m/z s in each PMF run are shown in Table S3.

45

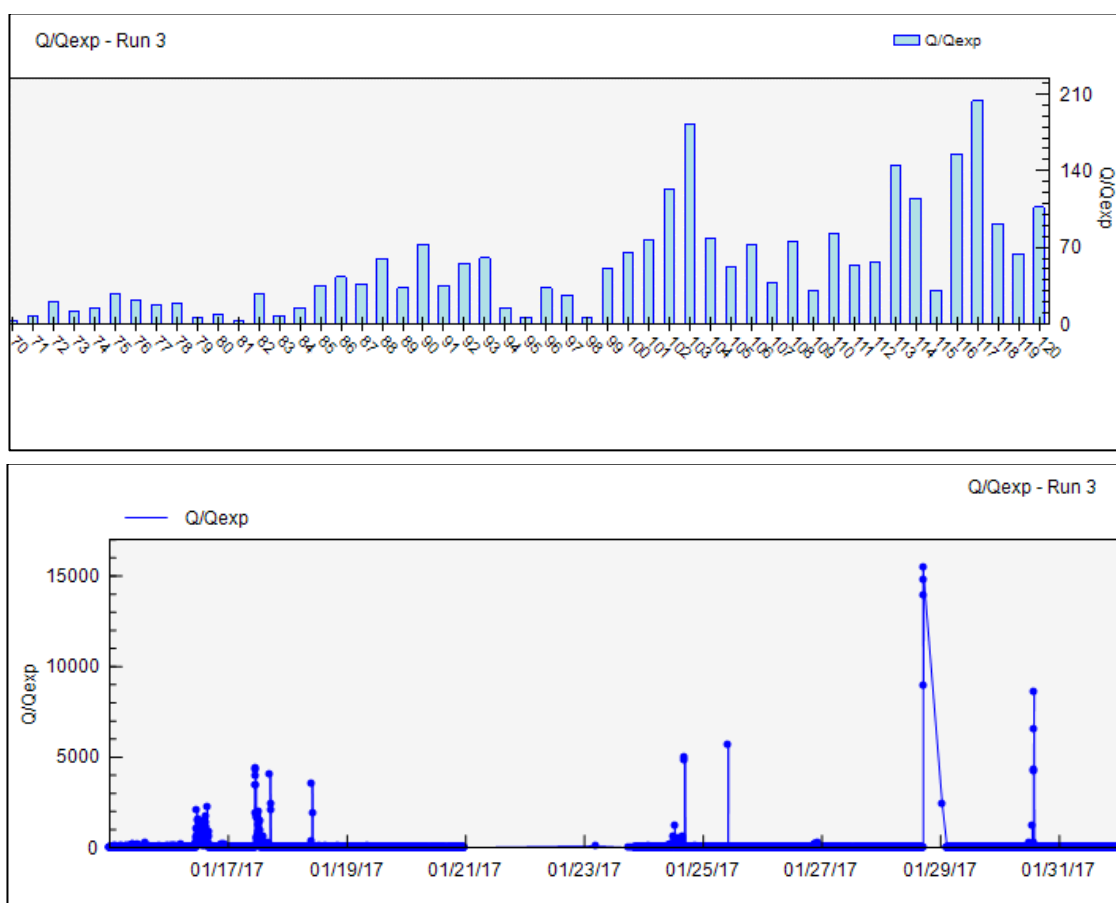


Figure S2 Q/Q_{exp} at (a) relevant time series points and (b) m/z s for raw organic data

As shown in Table S3, we identified important m/z s as either strong or weak in both the time-resolved and the seasonal PMF runs; thus, modeling error can be quantified by taking the difference of Q/Q_{exp} between two models (Paatero and Hopke,

50 2009). We used the default fragmentation table, and as a result, higher weight was given to mass spectral contribution at m/z 44, with which data at m/z values 16–18 is proportionally related. Accordingly, we down-weighted contributions at these m/z values and marked them as “weak”. To be consistent, identical trimmed parent organic data and error matrices were used between time-of-day PMF and seasonal PMF analyses. We conducted PMF runs for one to seven factors, explored the solution space using the tools FPEAK, seeds, and constraints, and conducted error analysis on the dataset. The IGOR PET tool, based on
55 PMF2, provides extensive information on different aspects of the residual structure in the tool itself (Ulbrich et al., 2009). However, the EPA PMF tool only generates .csv files that need to be individually analyzed for further analysis (Norris et al., 2014). An R package was developed to automate the process of data visualization and processing for subjective decision making by the PMF user (R Core Team, 2019). The package was based on libraries tidyverse (Wickham et al., 2019), openair (Carslaw et al., 2012), lubridate (Grolemund and Wickham, 2011), and MASS (Venables and Ripley, 2002).

60

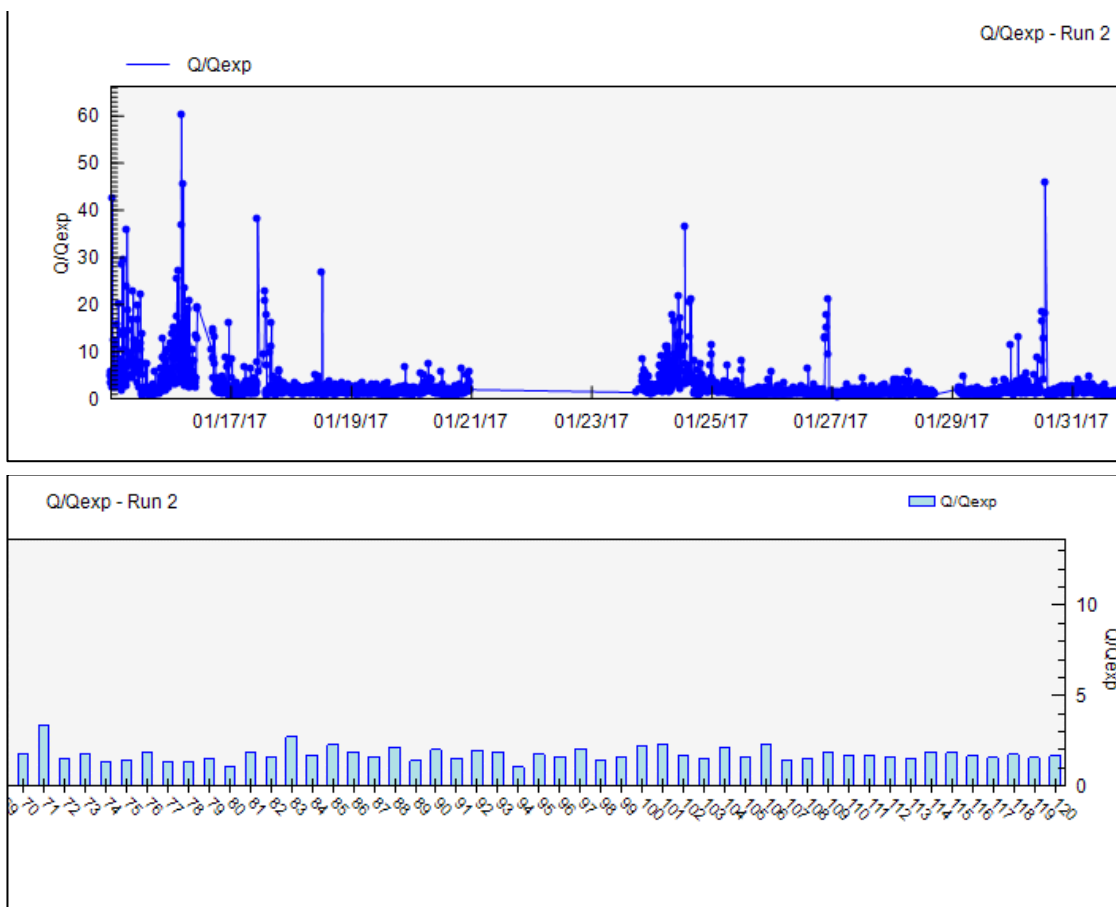


Figure S3 Q/Q_{exp} at relevant time series points and m/z s for trimmed organic data

Table S3 List of weak m/z s in PMF runs

Period	<i>m/zs</i>
W171115	13, 16–18, 24–25, 37–38, 44, 48–49, 62, 66, 75, 76, 80, 88–90, 92, 94, 100–104, 106, 108, 110, 112–114, 116–120
W172303	13, 15–18, 24, 37–38, 44
W17	13, 16–18, 24, 37–38, 44
M171115	13, 16–18, 24, 37, 44, 48–49, 61–62, 66, 72, 75, 80, 86–90, 92, 94, 98, 100–104, 106, 108, 110–114, 116–120
M172303	13, 16–18, 24–25, 37, 44, 48–49, 61–62, 75–76, 80, 87–90, 94, 100–104, 112–114, 116, 118, 120
M17	13, 16–18, 24, 37, 44, 48–49, 62, 66, 72, 75, 76, 80, 86–90, 94, 100–104, 108, 110, 112–114, 116, 118, 120

Table S4 Analyzed aspects of residual structure and criteria of factor selection

Aspect studied	Criteria of factor selection
Overall Q/Q_{exp} as a function of the number of factors	Q/Q_{exp} decreases as more factors are added. Here, we look at the rate of the drops as new solutions are added. After a few factor additions above two factors, the drops begin to stagnate to a constant. This is the point when new factors added explain minimal information in the residual structure.
Statistics of residual and scaled residual data	Mean values of Q/Q_{exp} may not be representative of other central tendencies and range of the Q/Q_{exp} distribution. Here, we look at the minimum, maximum, median, and histograms of Q/Q_{exp} to observe changes in residual structure. Small changes in the parameters and bleeding on the lower end of the histogram suggests optimal factor solution has likely been reached.
Correlogram of residual and scaled residual MS with reference MS profiles	The residual might be dominated by the influence of a specific PMF factor. Here, we look at correlations of residual MS with reference profiles to check if a specific type of factor dominates the residual MS, suggesting the addition of new factors might be needed.
Correlogram of residual TS with reference TS profiles	Mass spectral correlation of the residual MS with reference MS is not sufficient to attribute residual to a specific factor (Ulbrich et al., 2009). Here, we look at correlations of residual TS with external tracers to check if the specific type of factor identified in residual MS has relevant TS correlations with tracers.
Time series variations in residual and scaled residual patterns	Often, time series patterns by season, month of season, day of week, and hour of day can reveal information about factors due to similarity with human-activity patterns (Crippa et al., 2020). Here, we look at these patterns to identify changes in residual time series structure. As an example, a residual with minimal diurnal structure would be considered as more suitable than a residual with significant diurnal structure.
Q/Q_{exp} at different <i>m/zs</i>	Contributions at all <i>m/z</i> fragments are not equally fit. Here, we plot average Q/Q_{exp} at all <i>m/zs</i> and use the plot to identify transition points for fitting of data at <i>m/zs</i> , particularly those typically considered tracers, such as <i>m/zs</i> 29, 43, 44, 55, 57, 60, 73, and 115.

Time series variations in Q/Q_{exp}	Average values of overall Q/Q_{exp} cannot provide detailed information on the time series patterns of Q/Q_{exp} by season, month of season, day of week, and hour of day. These plots can reveal information about factors due to similarity with human-activity patterns (Crippa et al., 2020). Here, we look at these patterns to identify changes in Q/Q_{exp} time series structure. As an example, Q/Q_{exp} with minimal diurnal structure would be considered as more suitable than a residual with significant diurnal structure.
Range of scaled residuals at different m/z s	A large range of scaled residuals at different m/z s would suggest several time series points where the data does not fit contributions at these m/z s. We use this test as a check that the 25 th and the 75 th percentile of the scaled residuals at all m/z s are within ± 3 .

At the first step of analysis, we analyzed the improvement in the ability of the PMF solution to explain residual structure with the addition of factors. We selected an initial range of factors based on analysis of the residual structure. In this range, we selected an initial number of p factors based on correlations with the factors at the selection $p-1$. Specific aspects of the analyzed residual structure are included in Table S4. The next criteria employed for factor selection was the correlation of factor mass spectral profiles with reference mass spectra. We used as reference mass spectra the average mass spectral profiles developed by Ng et al. (2011) and cooking organic aerosol (COA) and coal combustion organic aerosol (CCOA) profiles in the AMS spectral databases (Ulbrich et al., 2017, 2018), and the one with the highest correlation with the mass spectrum of the PMF-generated factor (generally, Pearson $R \geq 0.9$) is used for naming the obtained factor (Ng et al., 2011). Other criteria employed to select the number of factors include the correlations of factor time series with external tracers, and time series patterns by season, month of season, day of week, and hour of day. As an example, we expected that the time series patterns would suggest high concentrations of BBOA in colder months and higher HOA at traffic hours in diurnal patterns. We extracted CO, NO₂, and O₃ data using the OpenAQ Platform (openaq.org, last access: 1 August 2019). The OpenAQ data originate from a fixed regulatory monitoring location, R.K. Puram, maintained by the Central Pollution Control Board (CPCB), government of India, about ~3–4 km aerial distance from the measurement site. This analysis marks the end of the second round of factor identification, with a selected number of factors. For correlations, we used the Pearson correlation coefficient (Pearson R) for mass spectral data and Spearman correlation coefficient (Spearman R) for time series patterns. This differentiation was recommended in the peer review of Ulbrich et al (2009), due to the limitation of Pearson R for slowly varying time series concentrations.

In previous work, differences between plausible factor solutions in the FPEAK–SEED 2-D space were considered representative of the uncertainty of the final selected solution (Ulbrich et al., 2009, Bhandari et al., 2020). We observed unreasonable MS, weak time series correlations, or rotational ambiguity on changing FPEAK and/or SEED from the default selection of FPEAK = 0 and SEED = 0. Therefore, default parameter values were used (Chapter 2; Bhandari et al., 2020). In EPA PMF, quantitative error estimation (EE) of random error and rotational ambiguity is conducted using BS, DISP, and BS-

DISP (Sect. 3.2.5). If the PMF factor solution passes all tests, BS, DISP, and BS-DISP, the solution was regarded as final. The statistical basis of these EE techniques is discussed in detail elsewhere (Paatero et al., 2014).

95 However, sometimes, the base PMF solutions did not pass uncertainty tests. To address the inability of the solution to pass the PMF tests, we changed the SEED value while keeping the number of factors constant. Changing the SEED value initializes the PMF algorithm with different pseudorandom starts. We changed the SEED value at least once and run 10 runs each time, leading to at least 20 random starts. If changing the SEED value did not lead to an improved base run, we either used FPEAK or applied constraints. Changing the FPEAK value allows exploring rotations of solutions of a given number of factors. We recalculate BS on running FPEAK to account for random errors; thus, FPEAK is particularly useful to improve
100 base solutions that pass the DISP test but fail BS. However, DISP and BS-DISP error evaluations are biased when FPEAK is used (Norris et al., 2014). Therefore, we rely on DISP of the base run; if the recalculated BS passes the threshold, we assumed that the issues associated with BS in BS-DISP would be fixed as FPEAK is used. We allow a 5% change in Q (or 5% d Q) relative to the base run in the solution obtained using FPEAK.

If changing FPEAK did not result in a better solution, we applied constraints on the solutions. Since reference profiles
105 are available, we used the “ratio” form of expressions for applying constraints. Application of constraints is very subjective; constraints were obtained from reference profiles, a cleaner factor in other periods, or a cleaner factor in a higher number of factors. Similar approaches have been used previously as well (Canonaco et al., 2015; Zhu et al., 2018; Tobler et al., 2020). To apply constraints, we identified the m/z s with the least uncertain contributions (Ng et al 2011). We combined the list of these m/z s with key m/z s such as m/z 29, 44, 43, 55, 57, 60, and 73. Application of constraints on some of these select m/z s
110 was sufficient to reach more optimal solutions, e.g., in some PMF runs, constraining the m/z 60 MS contribution to mean of the contribution in the reference profile moved the entire profile to a clean BBOA factor. We allowed a 5% change in Q (or 5% d Q) relative to the base run in the solution obtained by applying constraints. Despite the large d Q % allowed, factor profiles moved in the direction of the constraint but did not necessarily reach the exact value. This subjective movement of the profile allows generation of local profiles with tendencies reflected as similar to global profiles for the same factors.

115 **S2 Corrections to the EPA PMF code**

The EPA PMF tool references the work of Politis and White (2004) for estimating the bootstrap block size. However, in 2009, they published a correction to their bootstrap estimates (Patton et al., 2009). Updated source code for implementing the calculation of block size is also available (Hayfield and Racine, 2008). The code generates a block size based on each variable; thus, a subjective decision to select a single block size needs to be made. We base our decision for block size on the work of
120 Hemann and co-workers (2009). They apply the stationary block bootstrap approach for identification of block lengths. As a part of the process, we sum up the mass of all m/z s, find the optimal block length for that total mass, and compare the block length for total mass to block length for different percentiles of individual species. Next, we pick a block length that accounts for the total mass but also most of the individual species. Details of the block size calculations are shown in Table S5. In all cases, the used block size accounts for the total mass in PMF runs as well as more than 75% of contributions at different m/z s.

Period	Mean Block Size	Median Block Size	Block Size for total organics	Percentile Calculations		Used Block Size
				Percentile	Block Size	
W171115	36	36	42	90	43	43
W172303	53	53	53	100	54	54
M171115	94	94	97	90	98	98
M172303	98	99	100	75	100	100
M17	296	296	309	75	310	310
W17	160	160	161	90	162	162

Table S6 Steps for solution identification for specific EPA PMF runs

Period	Solution Identification
W171115	Residual analysis suggested 4–6 factor solutions. Factor swaps occurring in 5 and 6 factor solutions. Application of constraints at 5 and 6 factor solutions resulted in unreasonable MS or weak time series correlations. Base 4 factor solution fails BS test. Rotating the solution to FPEAK of 1 led to BS test resolution.
W172303	Residual analysis suggested 6–8 factor solutions. Attempted rotations and constraints for solutions with 6 or more factors but failed BS and DISP repeatedly. Base runs of 5 factor solutions fail DISP and show factor swaps at two or more factors, despite the application of rotations and constraints. Base runs of 4 factor solution fail BS at a semi-volatile oxidized OA factor, that shows mixing with HOA and BBOA factors. Constraining primary factors did not solve the problem. Rotations of the 4 factor solution allowed passing of the BS test but failed DISP. Finally, constraints based on the SVOOA reference profile were applied on the semi-volatile oxidized OA factor. Application of these constraints led to passing of all three tests.
W17	Residual analysis suggested 4–6 factor solutions. 5 and 6 factor solutions resulted in unreasonable MS or weak time series correlations. 4 factor solution fails BS-DISP test and shows factor swaps of BBOA, HOA, and local OOA factors. Constraining BBOA led to BS-DISP test resolution as well as improves BS mapping.
M171115	Residual analysis suggested 3–5 factor solutions. 4 and 5 factor solution resulted in unreasonable MS or weak time series correlations. 3 factor solution base run passes all tests.
M172303	Residual analysis suggested 3–5 factor solutions. 5 factor solutions resulted in two factors with no time series correlations. 4 factor solution passes DISP and BS-DISP tests but fails BS test. Rotating solution to FPEAK 15 led to the necessary improvement in BS mapping.
M17	Residual analysis suggested 3–5 factors. 4 factors and above gave identical TS correlations at multiple factors.

Table S7 Details of number of factors, seed, constraints, rotations applied in EPA PMF

Period	Solution Identification
--------	-------------------------

W171115	4 factor solution at seed 83 was rotated to FPEAK 1
W172303	4 factor solution at seed 6 was constrained with SVOOA presence at factor 3
W17	4 factor solution at seed 5 was constrained with BBOA presence at factor 1
M171115	3 factor solution at seed 76 with no constraints or rotations applied
M172303	4 factor solution at seed 54 was rotated to FPEAK 15
M17	3 factor solution at seed 83 with no constraints or rotations applied

130

Table S8 BS mapping results (reported in terms of BS mapping observed in period)

Period	Factors Separated in EPA PMF	BS Mapping (out of 100)
W171115	SFC-OA, BBOA, Local OOA, Regional OOA	100, 92, 100, 95
W172303	HOA, BBOA, Local OOA, Regional OOA	100, 99, 97, 100
W17	HOA, BBOA, Local OOA, Regional OOA	100, 100, 100, 100
M171115	POA, Local OOA, Regional OOA	95, 77, 100
M172303	HOA, COA, Local OOA, Regional OOA	100, 100, 96, 99
M17	POA, Local OOA, Regional OOA	NA ^a

^aTest terminated prematurely due to large computational size of data

Table S9 DISP swap performance results for lowest dQ -max

Period	Factors Separated in EPA PMF	DISP Swaps
W171115	SFC-OA, BBOA, Local OOA, Regional OOA	0, 0, 0, 0
W172303	HOA, BBOA, Local OOA, Regional OOA	0, 0, 0, 0
W17	HOA, BBOA, Local OOA, Regional OOA	0, 0, 0, 0
M171115	POA, Local OOA, Regional OOA	0, 0, 0
M172303	HOA, COA, Local OOA, Regional OOA	0, 0, 0, 0
M17	POA, Local OOA, Regional OOA	0, 0, 0, 0

135

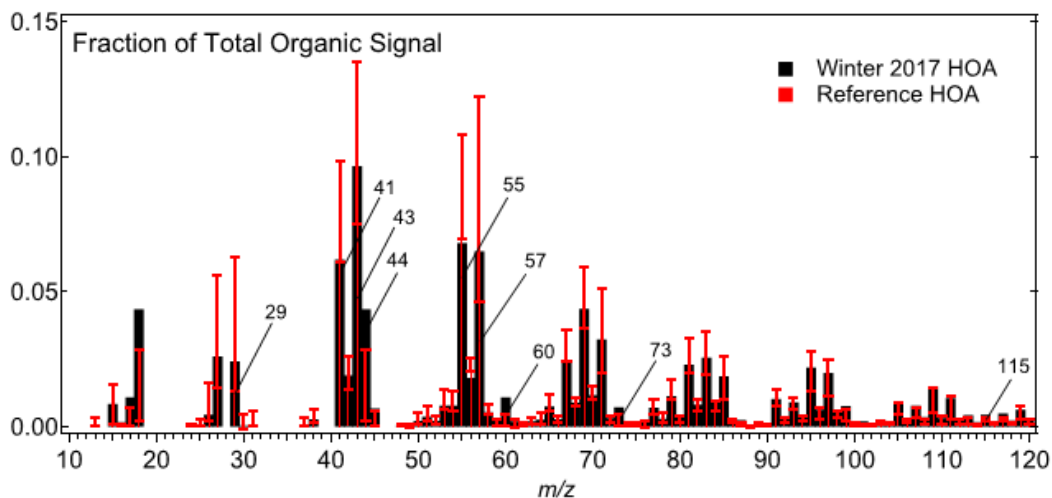
Table S10 BS-DISP swap performance results for lowest dQ -max

Period	Factors Separated in EPA PMF	Accepted Cases	BS-DISP Swaps
W171115	SFC-OA, BBOA, Local OOA, Regional OOA	82	2, 1, 0, 3
W172303	HOA, BBOA, Local OOA, Regional OOA	NA ^a	0, 0, 0, 0

W17	HOA, BBOA, Local OOA, Regional OOA	83	11, 7, 4, 0
M171115	POA, Local OOA, Regional OOA	98	0, 0, 0
M172303	HOA, COA, Local OOA, Regional OOA	93	1, 1, 0, 0
M17	POA, Local OOA, Regional OOA	NA ^b	NA

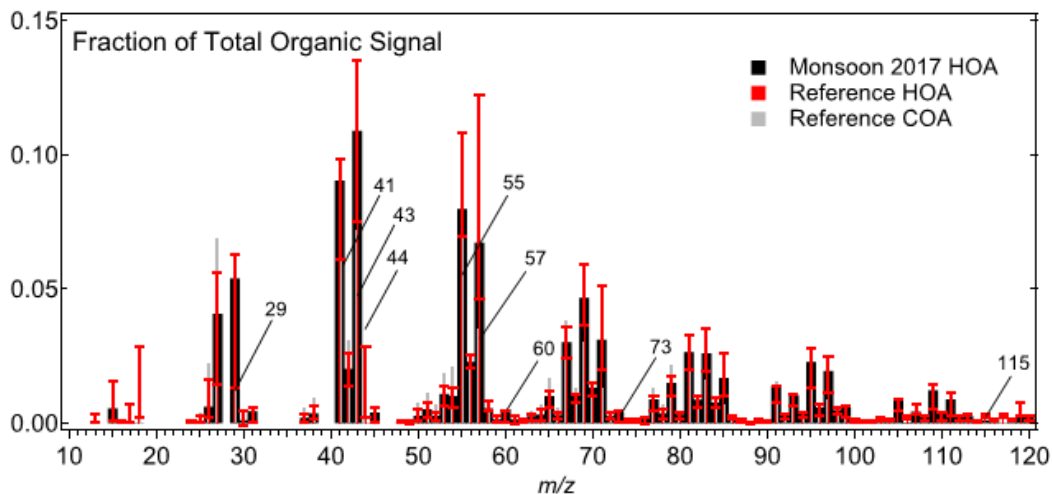
^aTest terminated prematurely due to unknown cause

^bTest terminated due to large computational size of data



140

Figure S4 shows mass spectrum of seasonal PMF primary organic aerosol (POA) factor in winter 2017. The whiskers in the graphs represent ± 1 standard deviation (SD) of the reference spectra. The mass spectrum resembles the reference HOA profile.



145

Figure S5 shows mass spectrum of seasonal PMF primary organic aerosol (POA) factor in monsoon 2017. The whiskers in the graphs represent ± 1 SD of the reference spectra. The mass spectrum resembles the reference HOA profile.

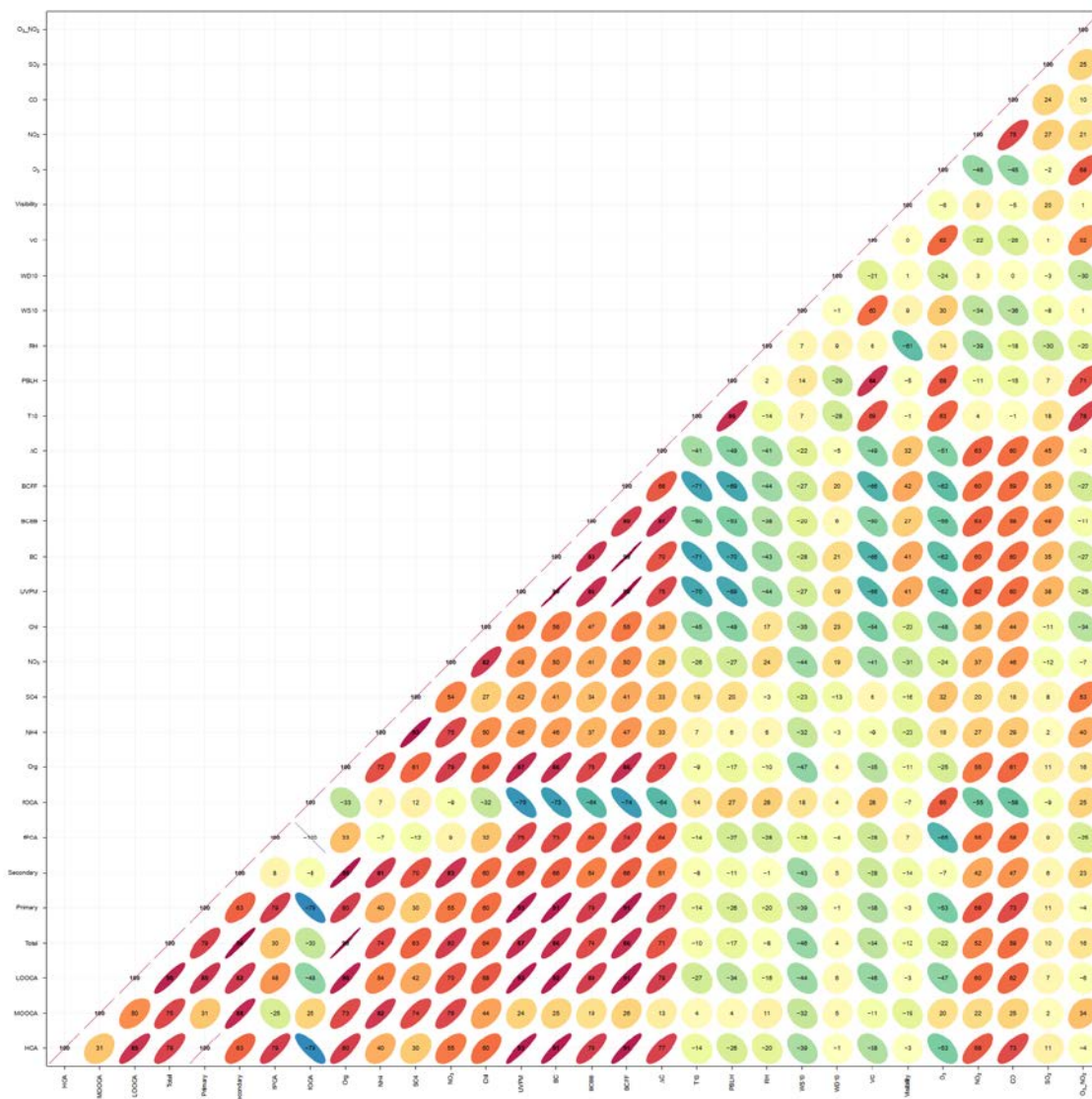


Figure S6 shows the time series correlations of the seasonal PMF factors' TS and their fractions' TS with external tracers for the season of monsoon 2017 (for expanded figure, see Supplementary File-FigS6).

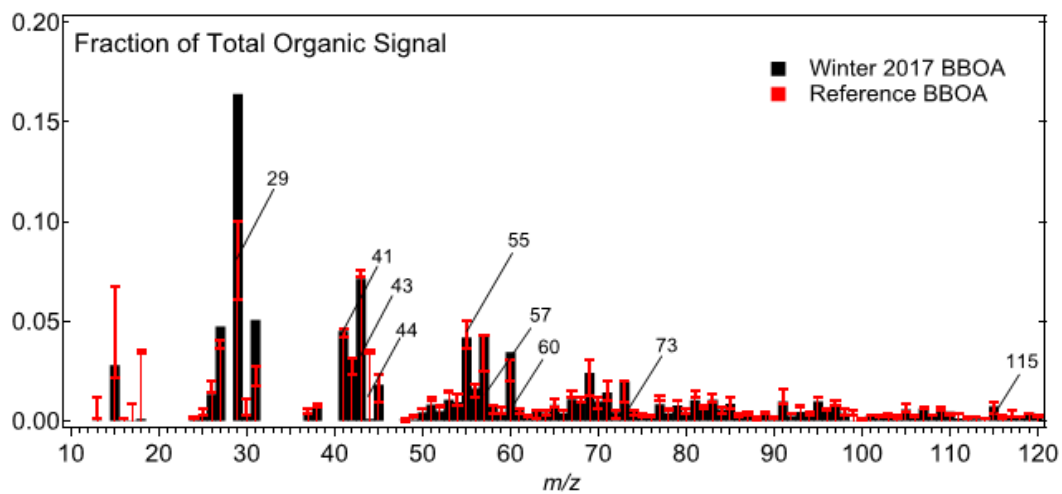


Figure S7 shows mass spectrum of seasonal PMF biomass burning organic aerosol (BBOA) factor in winter 2017. Whiskers in the graphs represent ± 1 SD of the reference spectra. The mass spectrum resembles the reference BBOA profile.

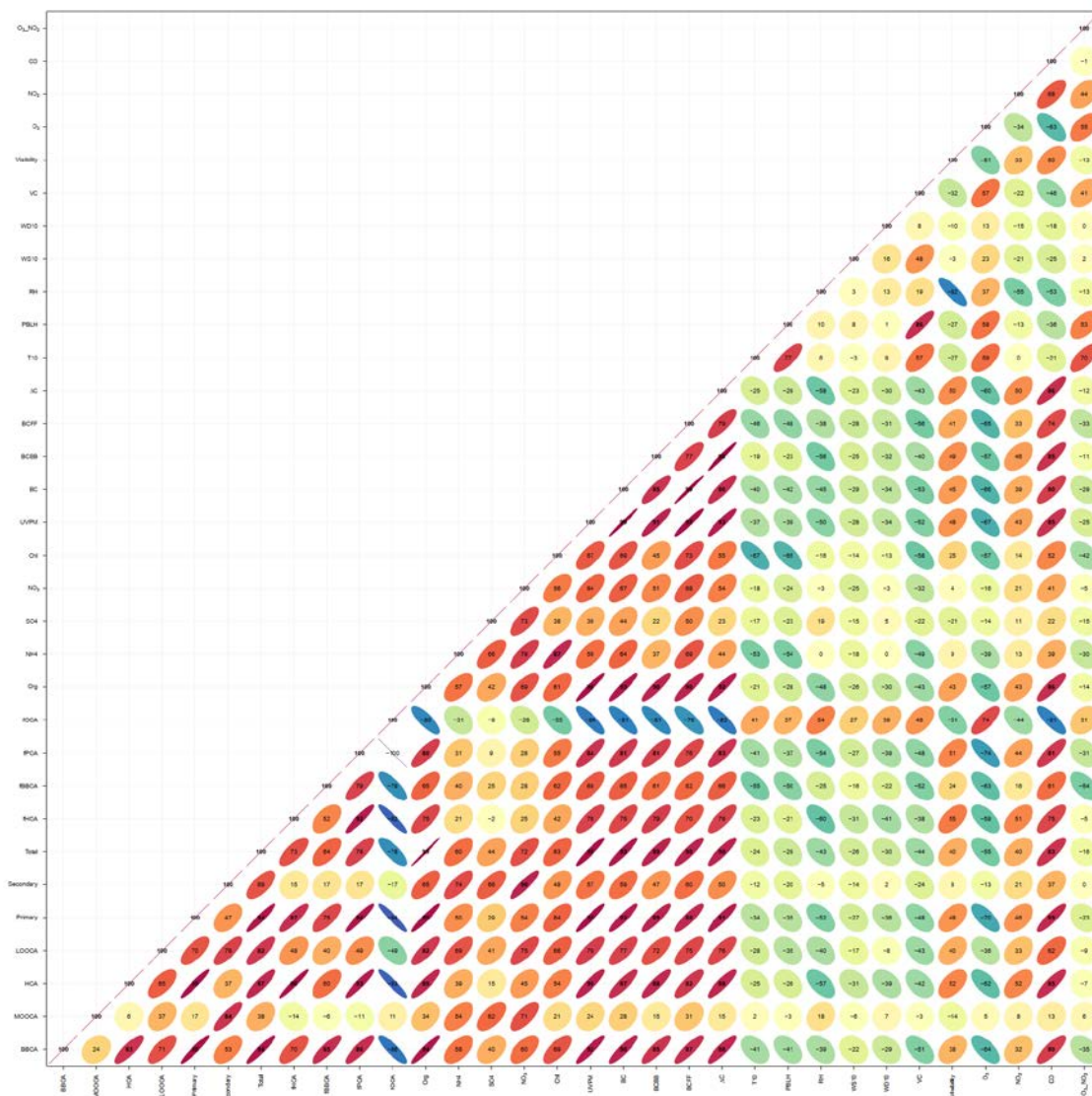
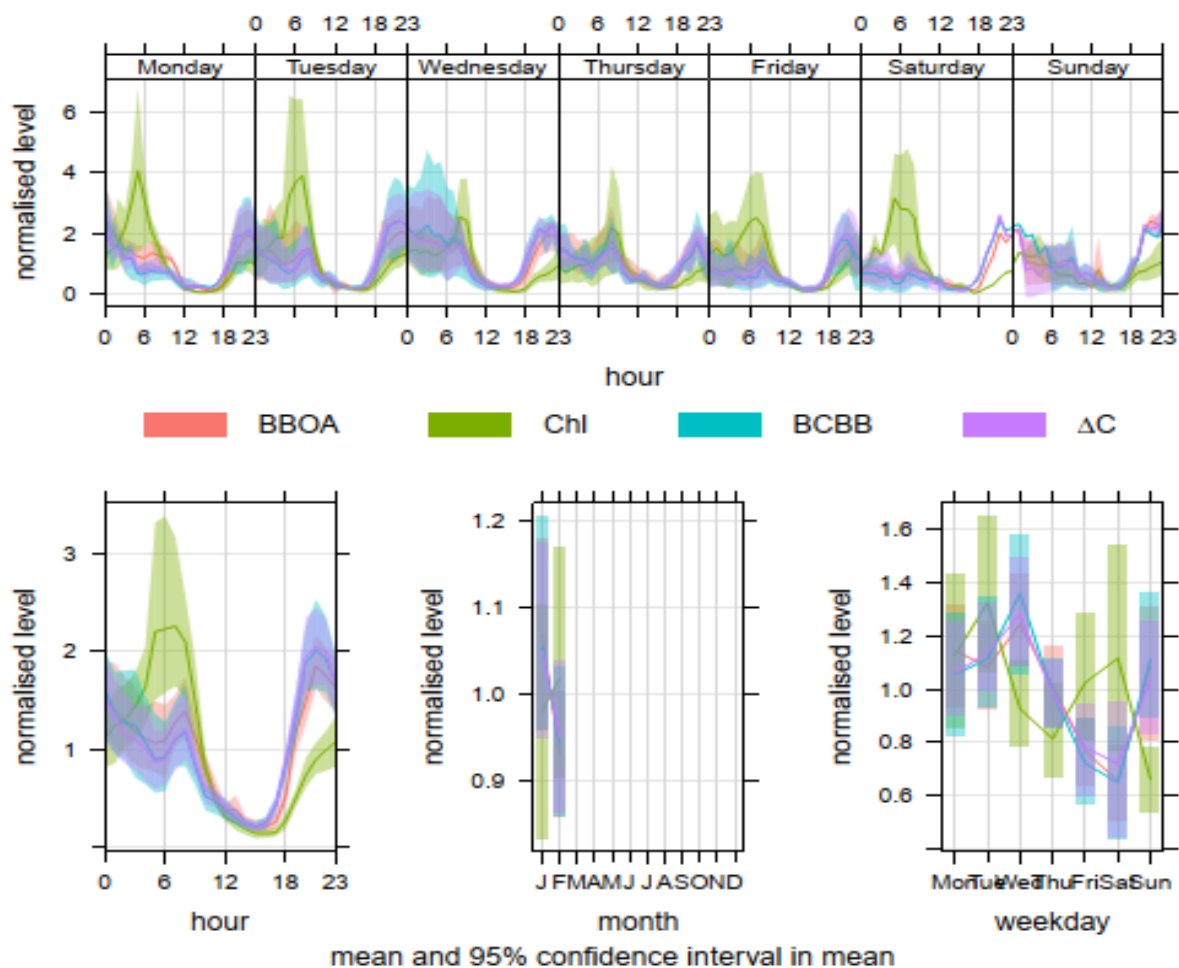
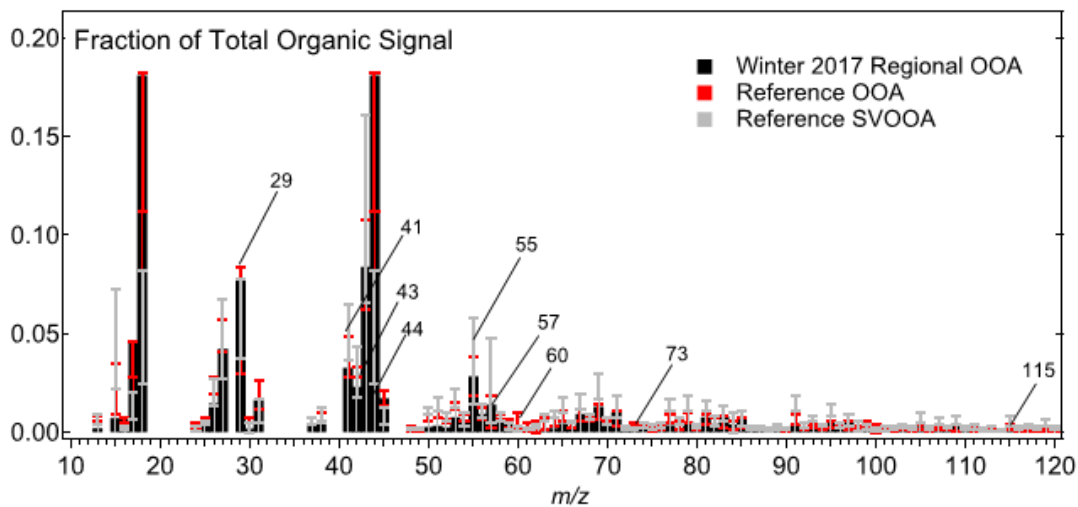
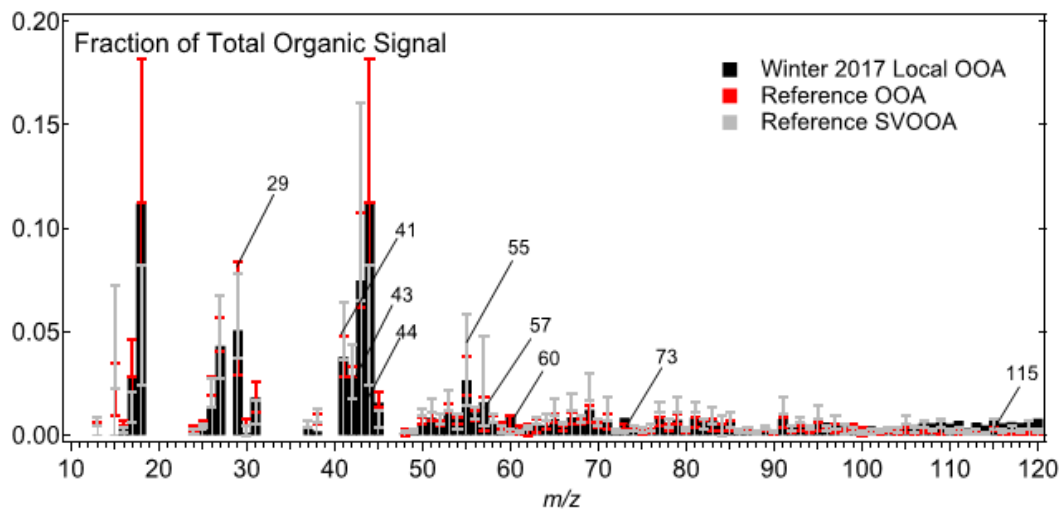


Figure S8 shows the time series correlations of the seasonal PMF factors' TS and their fractions' TS with external tracers for the season of winter 2017 (for expanded figure, see Supplementary File-FigS8).



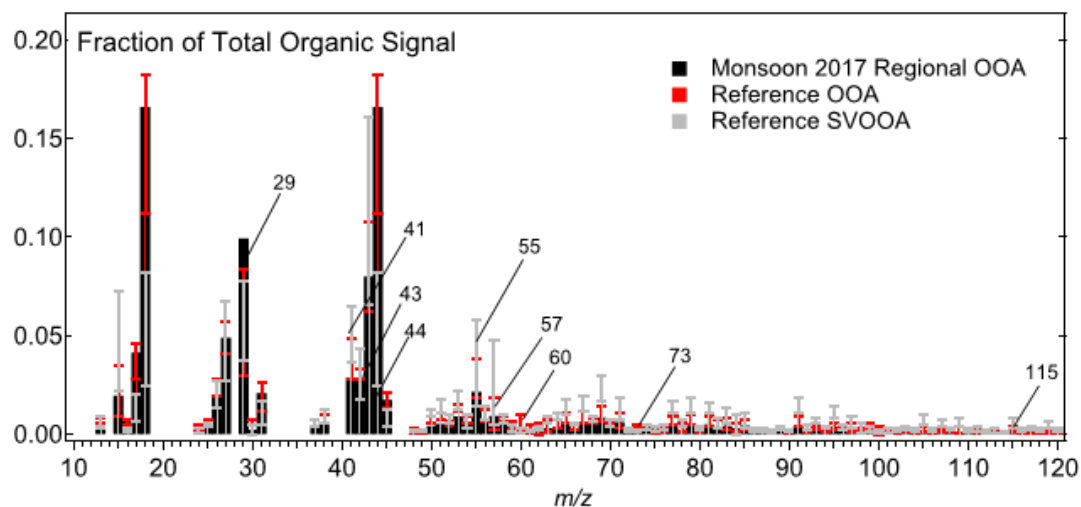
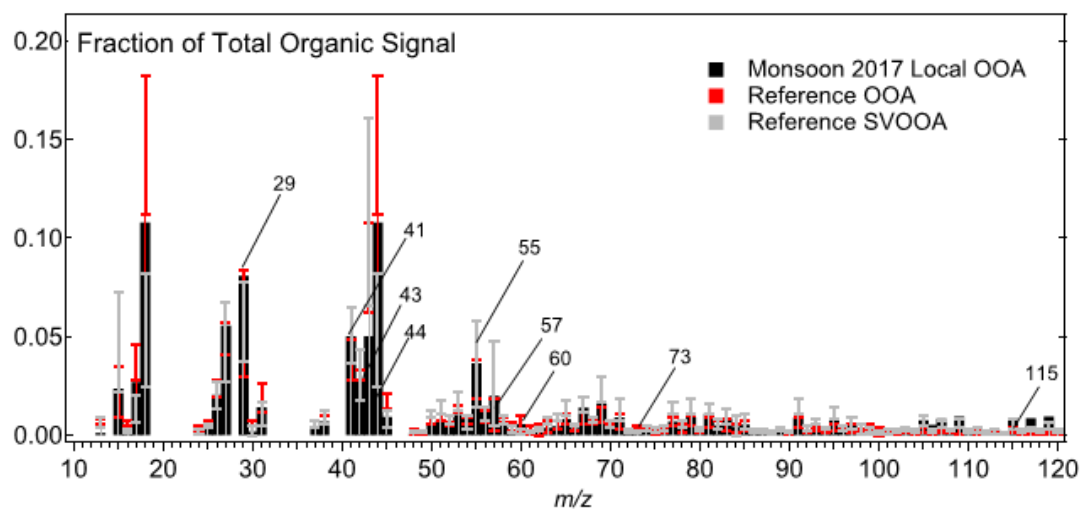
165

Figure S9 shows the hour-of-day on the day-of-week, seasonal diurnal, monthly, and week-of-day time series patterns for BBOA, chloride, BC_{BB}, and ΔC for the seasonal PMF run of winter 2017.



170 Figure S10 shows the mass spectrum of seasonal PMF oxidized organic aerosol (OOA) factors: (a) local OOA and (b) regional OOA in winter 2017. Both MS are similar to the reference OOA factor. The whiskers in the graphs represent ± 1 SD of the reference spectra. The two MS are at the two extremes for the range of contributions at m/z 44, pointing to the different oxidation state of aerosols.

175



180 Figure S11 shows the mass spectrum of seasonal PMF oxidized organic aerosol (OOA) factors: (a) local OOA and (b) regional OOA in monsoon 2017. Both MS are similar to the reference OOA factor. The whiskers in the graphs represent ± 1 SD of the reference spectra. The two MS are at the two extremes for the range of contributions at m/z 44, pointing to the different oxidation state of aerosols.

185

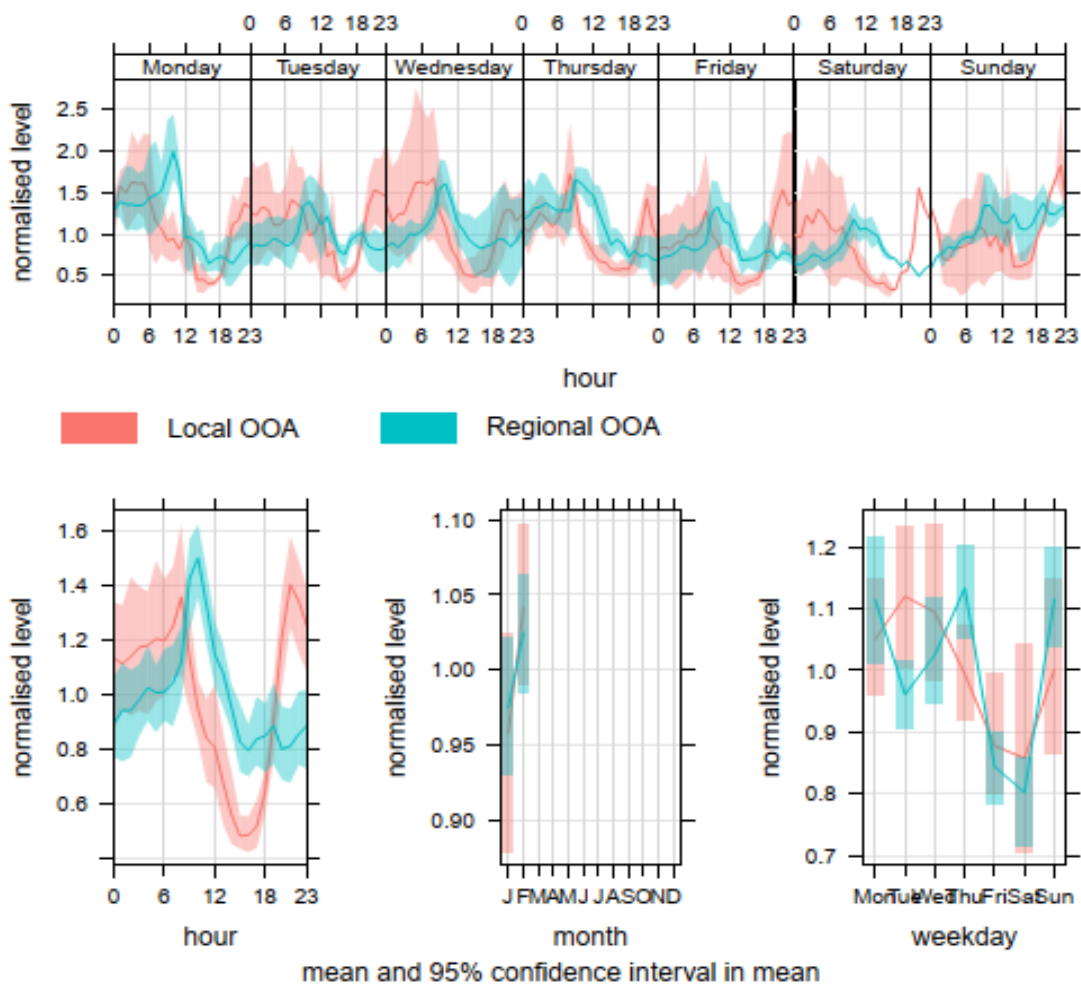
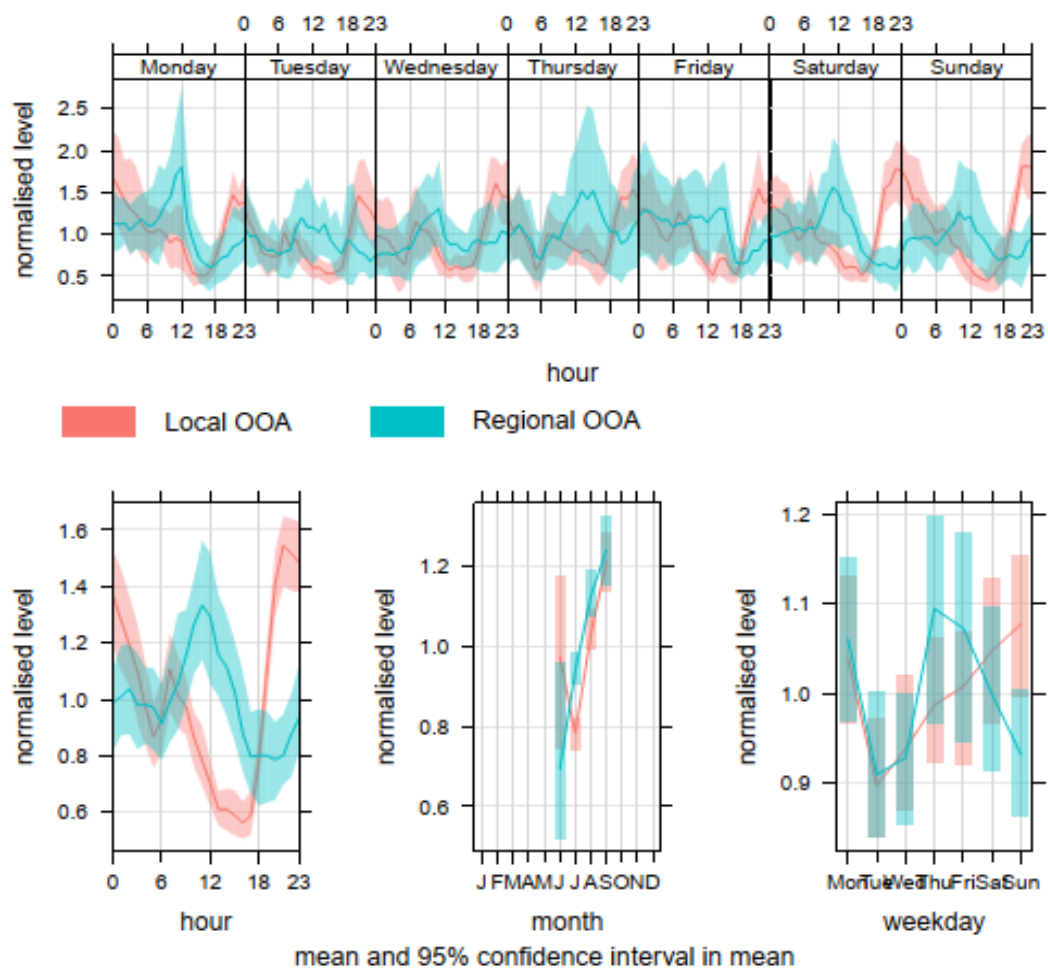


Figure S12 shows the hour-of-day on the day-of-week, seasonal diurnal, monthly, and week-of-day time series patterns for local OOA and regional OOA for the seasonal PMF run of winter 2017. Clearly, regional OOA is less variable diurnally than local OOA.

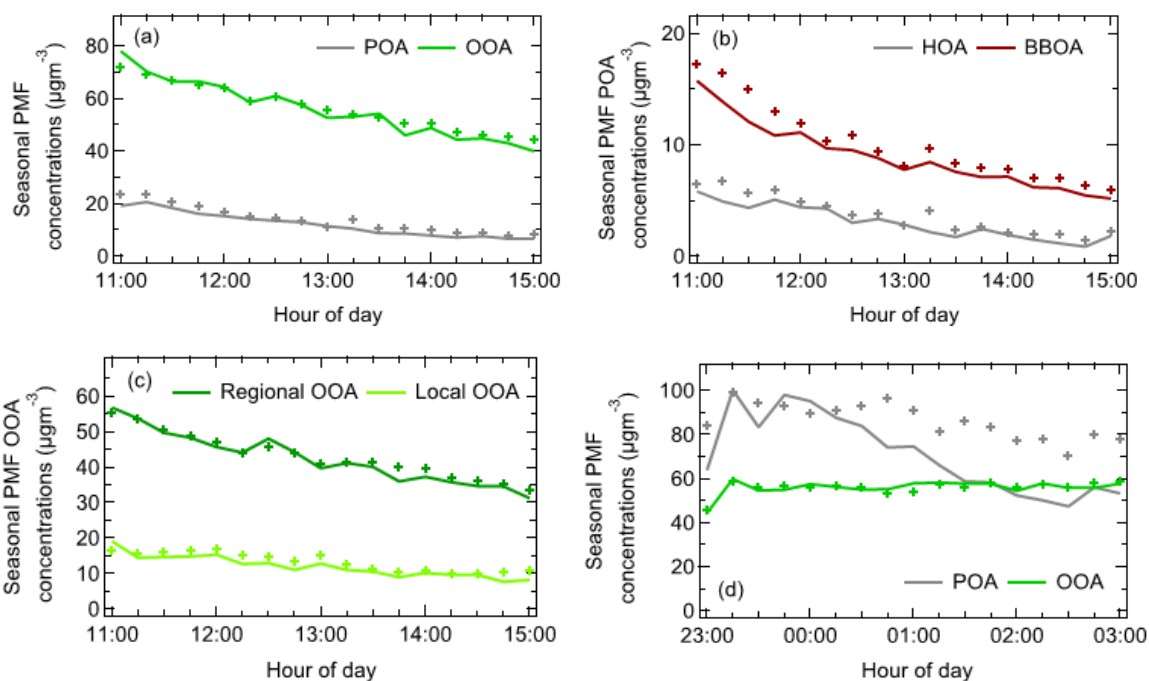


195 Figure S13 shows the hour-of-day on the day-of-week, seasonal diurnal, monthly, and week-of-day time series patterns for local OOA and regional OOA for the seasonal PMF run of monsoon 2017. Clearly, regional OOA is less variable diurnally than local OOA.

200

S3 Detailed 15 min time series patterns of seasonal PMF factors at midday and nighttime

205 Time series patterns exhibit contrasting behavior in winter and monsoon. In winter, seasonal PMF POA time series patterns exhibit strong variability midday but remain relatively stable at nighttime (Fig. S14a–f). At winter midday, concentrations of both HOA and BBOA exhibit a monotonically decreasing pattern. In this period, winter peak HOA and BBOA concentrations are ~ 6 and ~ 3 times the period minimum, respectively (Figs. S14b–c). At winter night, concentrations of HOA and BBOA are higher than midday by a factor of ~ 14 and ~ 4 , respectively, and are comparatively stable; peak concentrations at night are only ~ 2 times the period minimum (Figs. S14e–f). In contrast, monsoon POA exhibits relatively stable midday (peak POA ~ 2 times the period minimum) and variable nighttime (peak POA ~ 3 times the period minimum) patterns, with nighttime concentrations higher than midday by a factor of ~ 3.5 (Fig. S15a, c). These dynamics could be explained by the differences in ventilation coefficient, source strength, reaction chemistry, and the effect of temperature on partitioning (Bhandari et al, 2020). The large mean–median difference in POA factors suggests the influence of episodes. Compared to POA, OOA time series patterns are relatively stable (Figs. S14c, f). In winter midday, the local OOA factor (peak OOA ~ 2.5 x period minimum) has a stronger variability than the regional OOA factor (peak OOA ~ 2 x period minimum), but the OOA factors both show a similar monotonically decreasing trend (Fig. S14c). At winter night, we observe no trends in OOA factors (Fig. S14f). Monsoon OOA factors show behavior similar to POA factors (Fig. S15b, d). Local and regional OOA midday and at nighttime exhibit very limited variability (peak OOA ≤ 1.5 x period minimum).



220

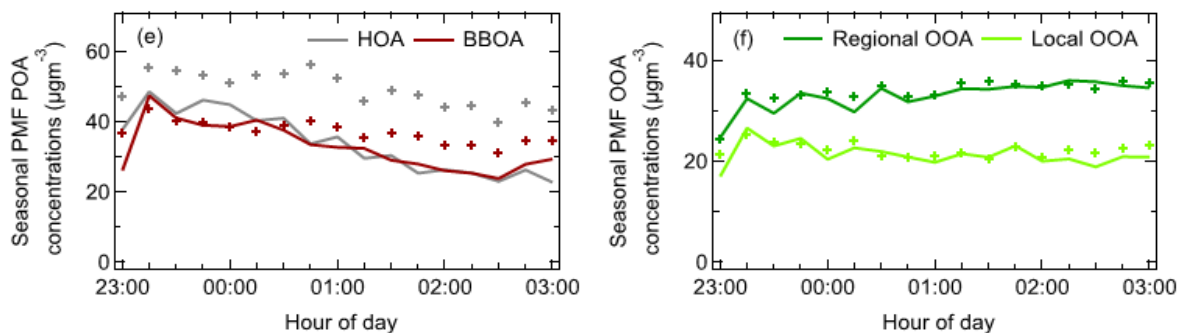


Figure S14 shows 15 min averaged seasonally representative concentration time series of seasonal PMF factors for the periods: (a)-(c) W171115 and (d)-(f) W172303. nighttime POA factors show stronger evidence of episodes (in $\mu\text{g m}^{-3}$).

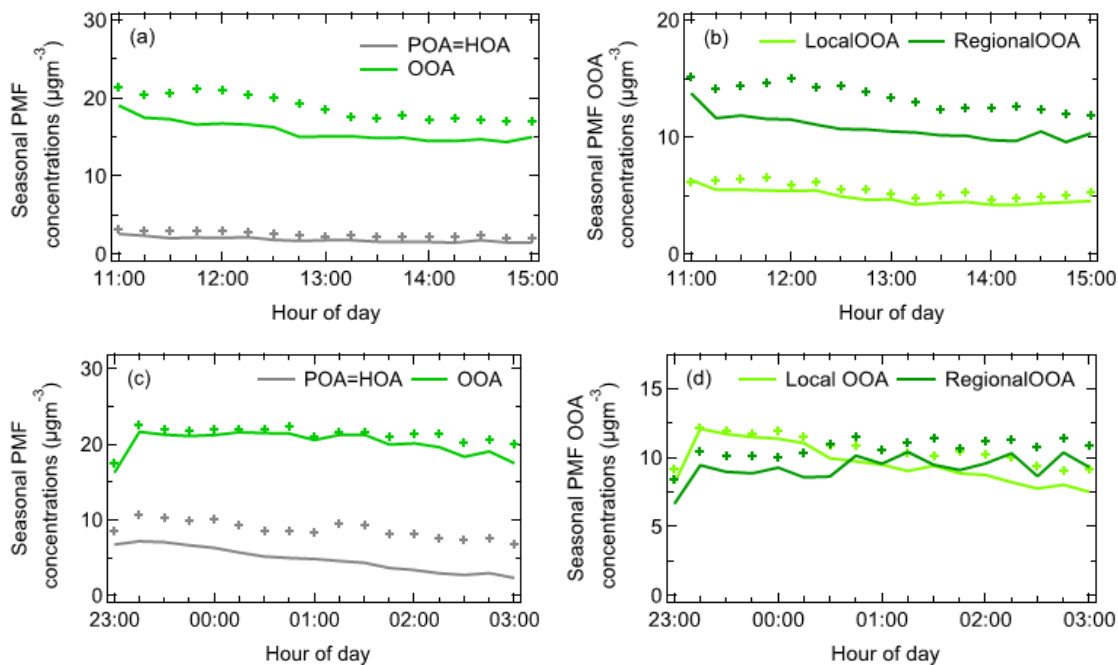
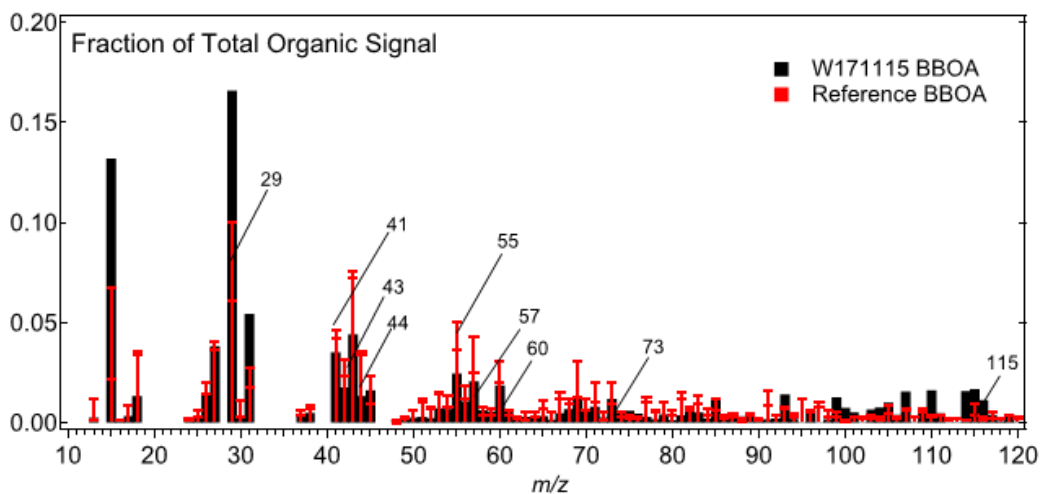
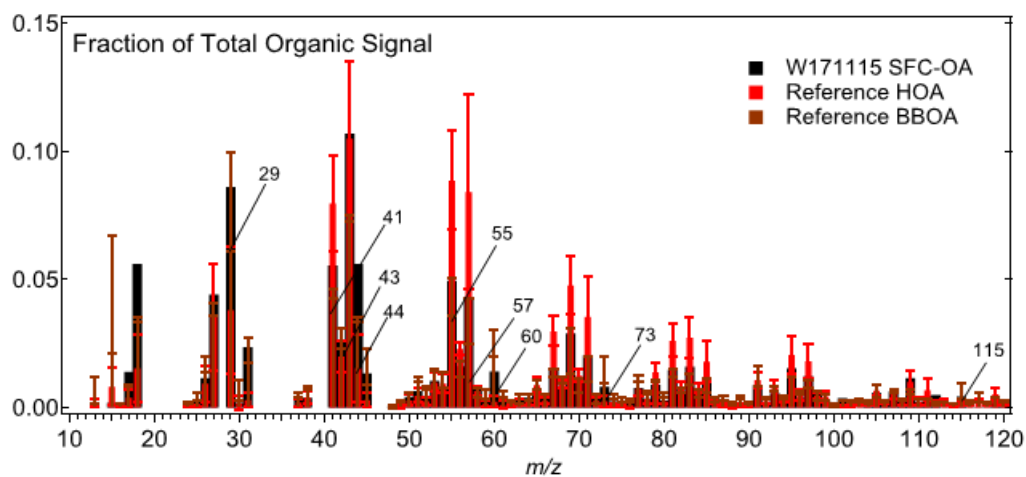


Figure S15 shows 15 min averaged seasonally representative concentration time series of seasonal PMF factors for the periods: (a)-(b) M171115 and (c)-(d) M172303. nighttime POA factors show stronger evidence of episodes (in $\mu\text{g m}^{-3}$).

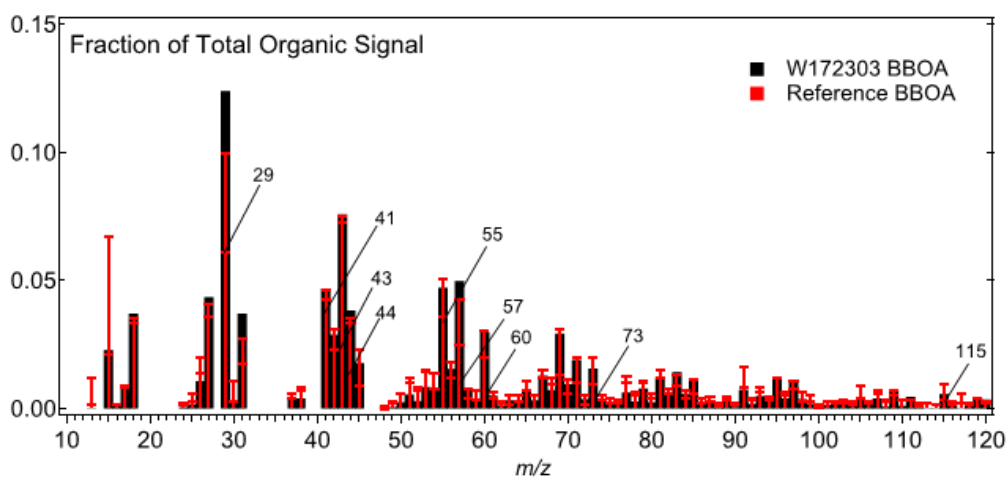
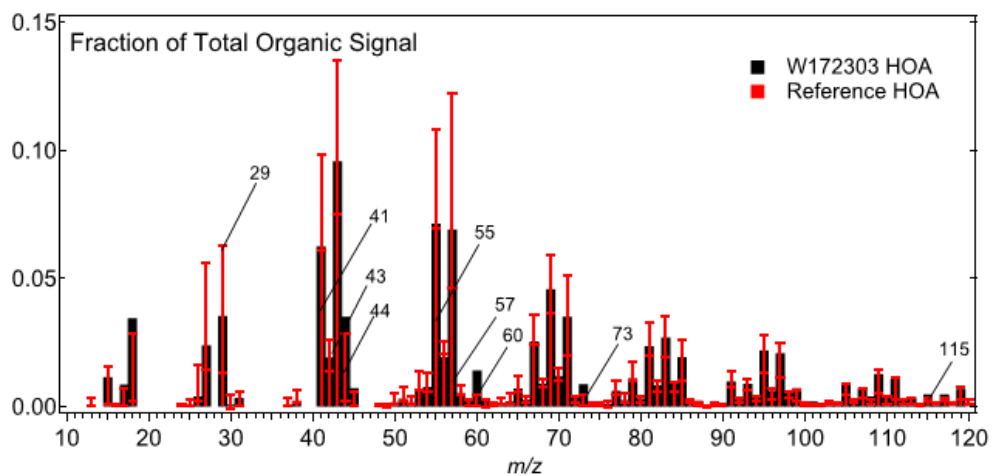
225

230

235

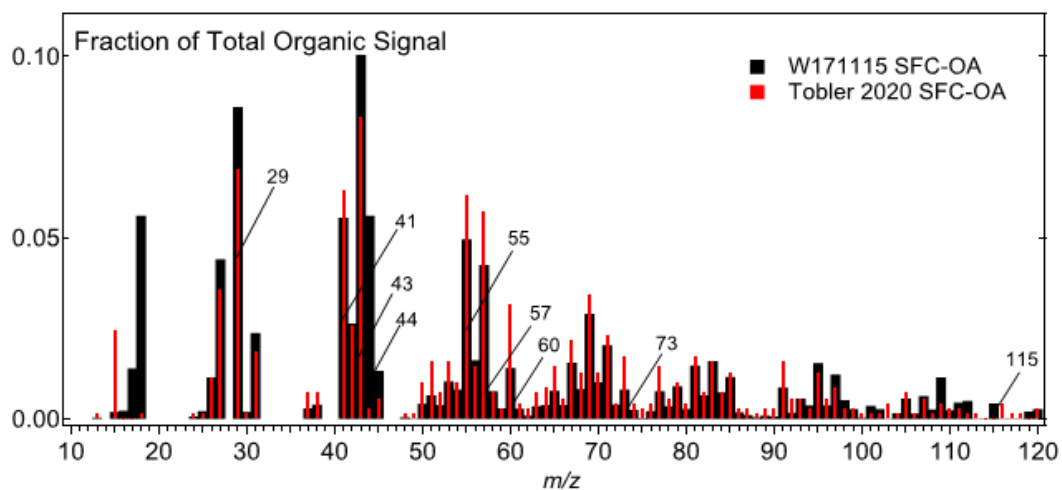


240 Figure S16 shows the mass spectrum of time-of-day PMF primary OA factors: (a) W171115 SFC-OA and (b) W171115 BBOA at winter midday in 2017. The whiskers in the graphs represent ± 1 SD of the reference spectra. W171115 SFC-OA MS shares similarities with both reference HOA and BBOA MS. W171115 BBOA MS has higher m/z 29 and lower m/z 60 than reference BBOA MS.

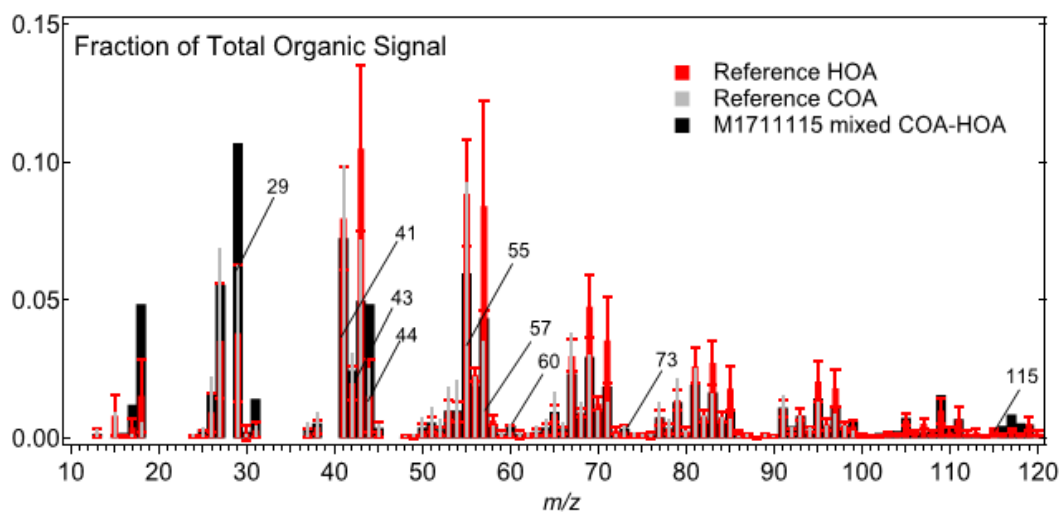


245

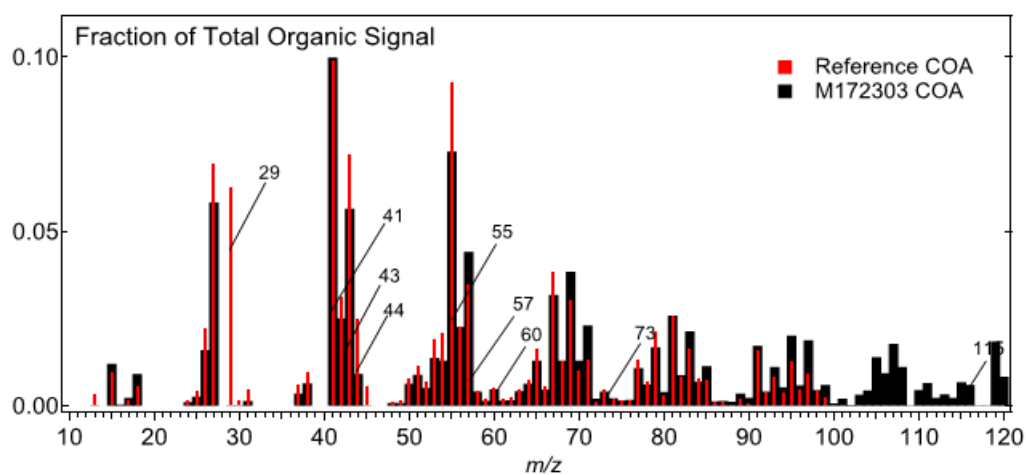
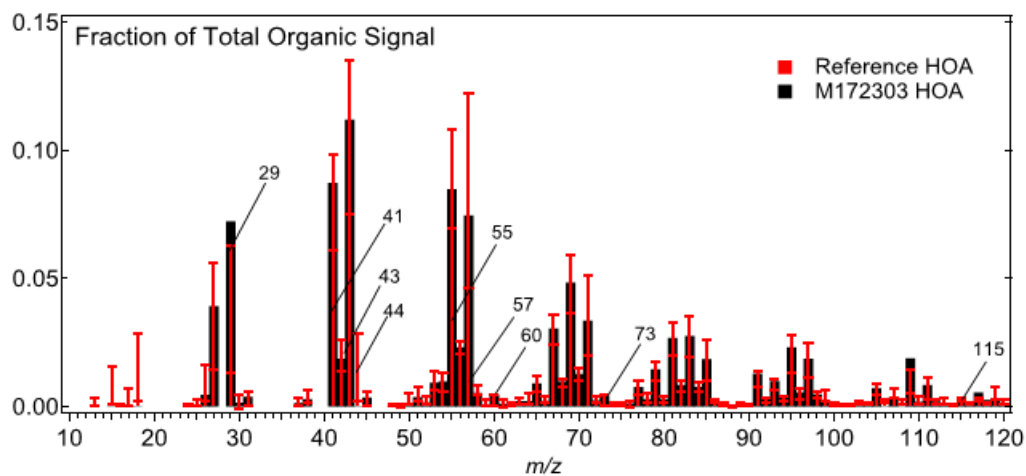
Figure S17 shows the mass spectrum of time-of-day PMF primary OA factors: (a) W172303 HOA and (b) W172303 BBOA at winter nighttime in 2017. The whiskers in the graphs represent ± 1 SD of the reference spectra. W172303 HOA MS is similar to the reference HOA MS. W172303 BBOA MS is similar to reference BBOA MS.



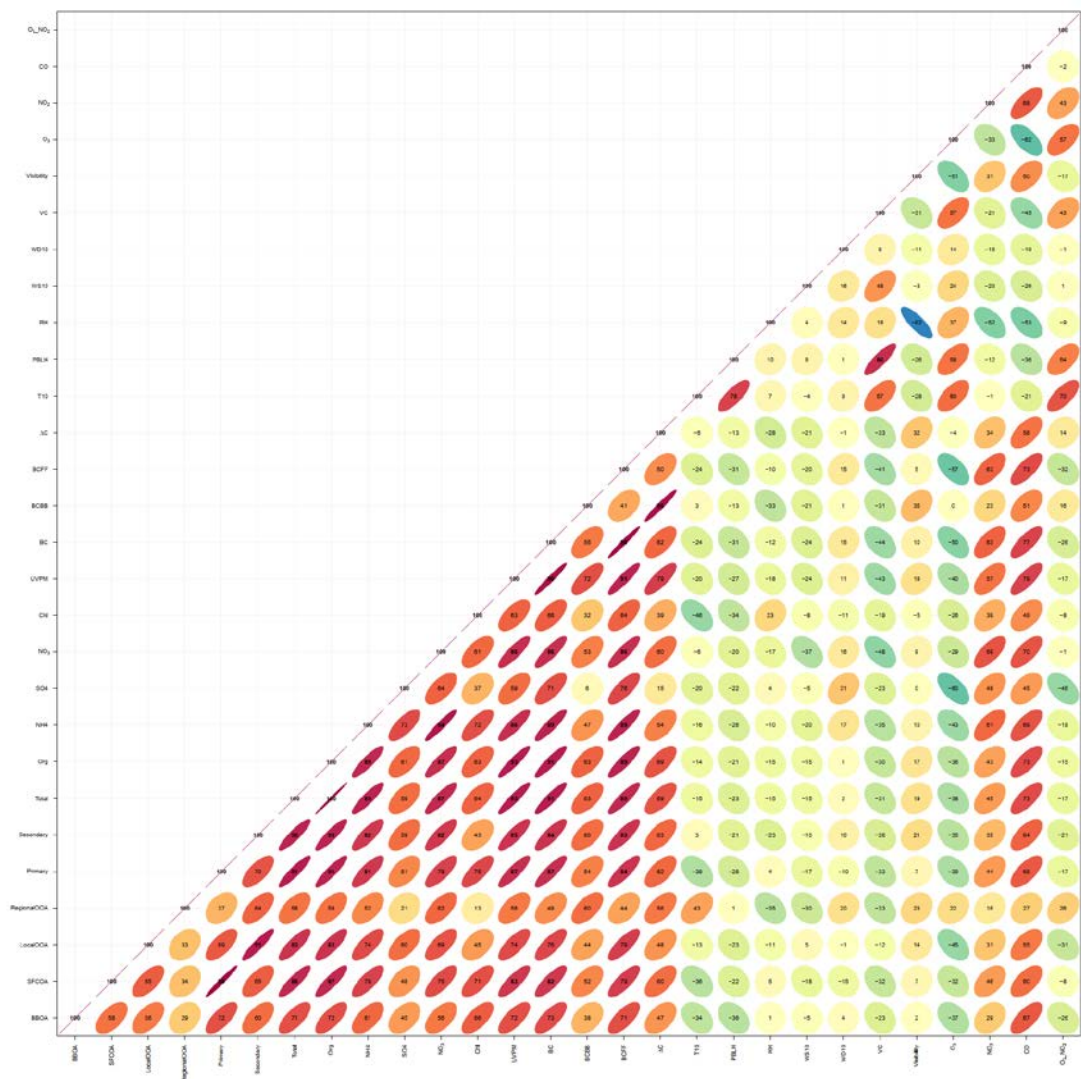
250 Figure S18 shows the mass spectrum of time-of-day PMF primary OA factor W171115 SFC-OA at winter midday in 2017 and the SFC-OA profile from the work of Tobler and co-workers (2020). MS contributions are very similar except at m/z 44.



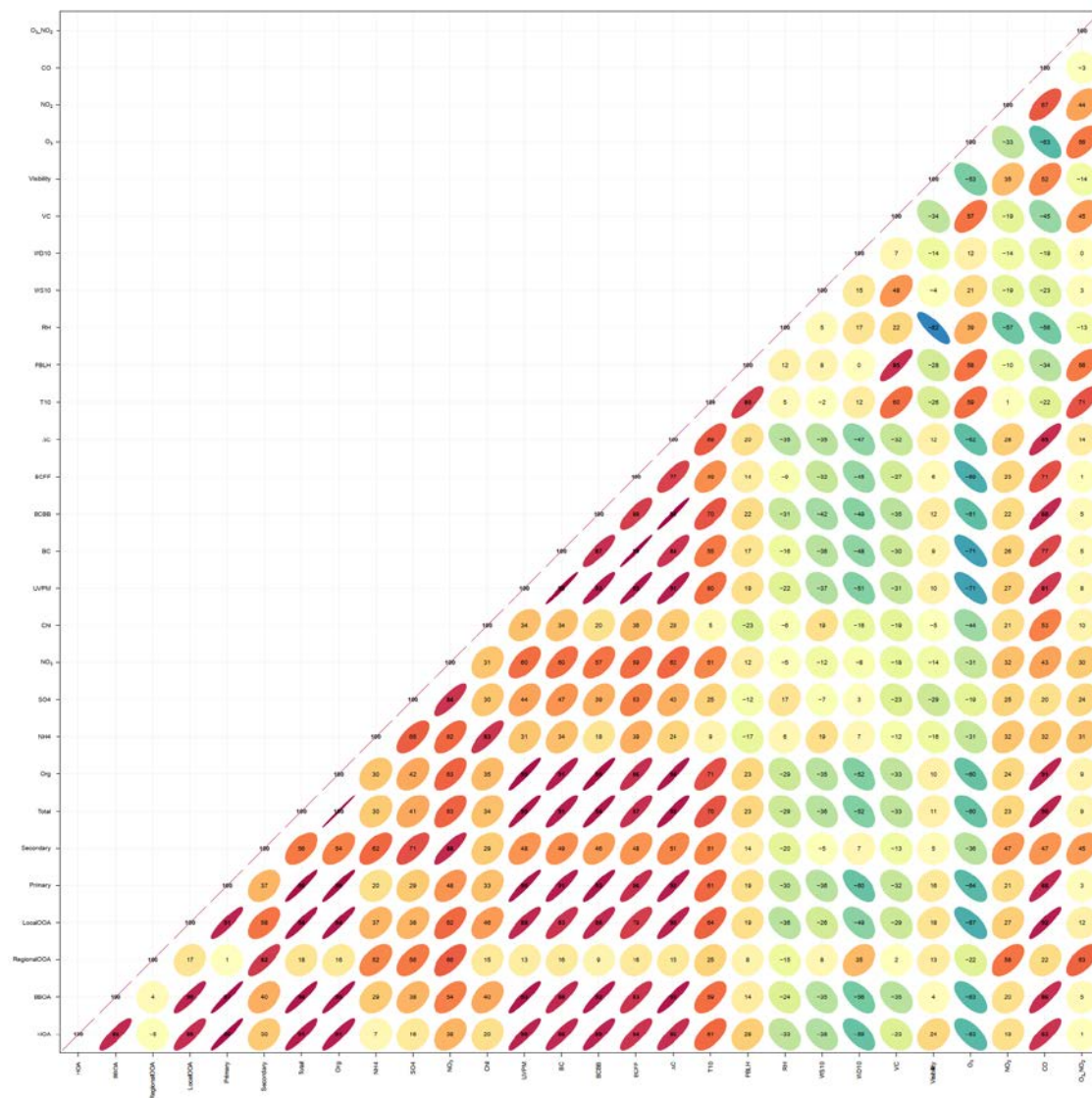
255 Figure S19 shows the mass spectrum of time-of-day PMF primary OA factor M171115 mixed COA-HOA at monsoon midday in 2017. The whiskers in the graphs represent ± 1 SD of the reference spectra. M171115 COA-HOA MS shares similarities with both reference HOA and COA MS.



260 Figure S20 shows the mass spectrum of time-of-day PMF primary OA factors: (a) M172303 HOA and (b) M172303 COA at monsoon nighttime in 2017. The whiskers in the graphs represent ± 1 SD of the reference spectra. M172303 HOA MS is similar to the reference HOA MS. M172303 COA MS is similar to reference COA MS.

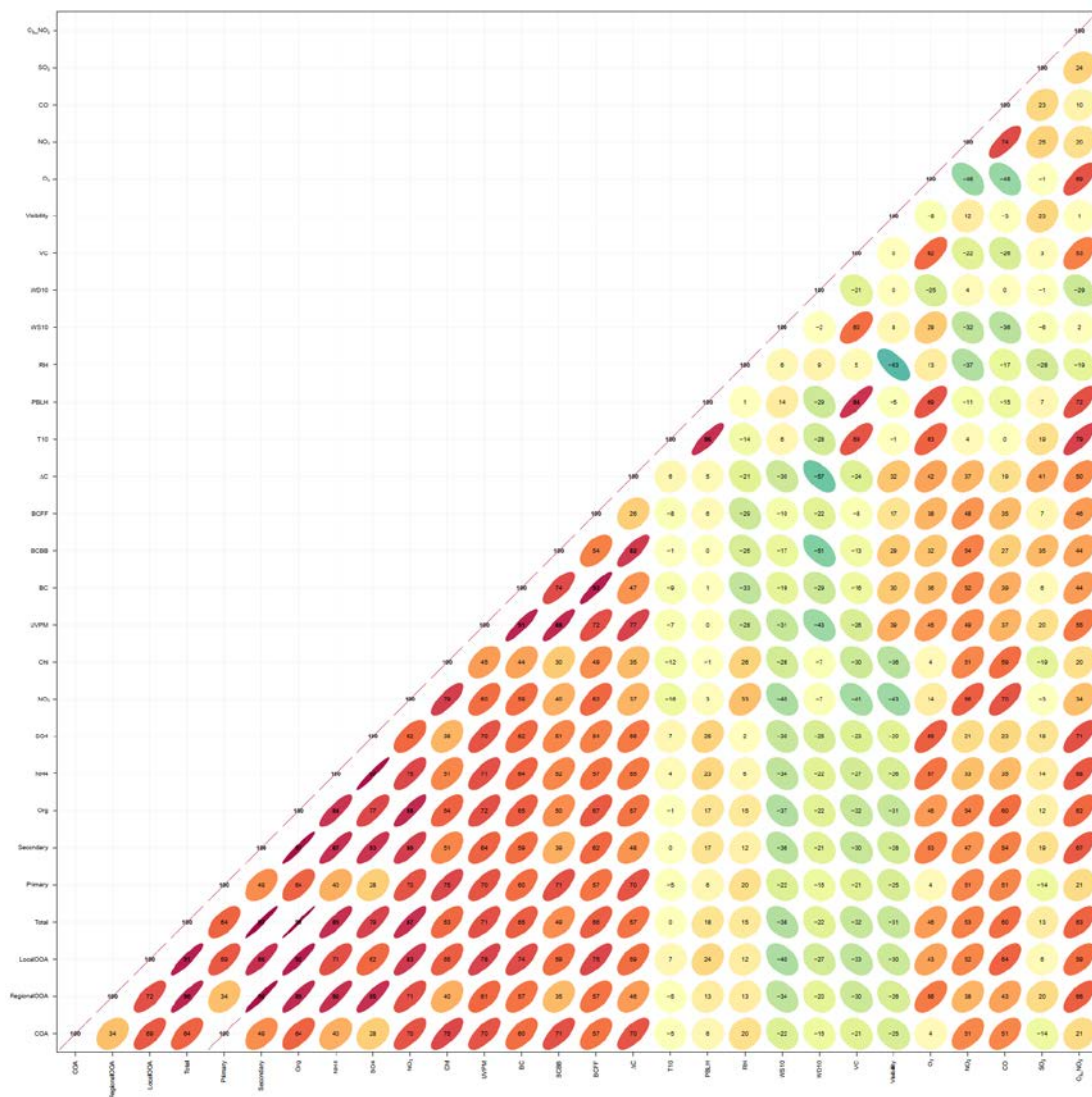


265 **Figure S21** shows the time series correlations of the PMF factors' TS with external tracers for the period of W171115 (for expanded figure, see Supplementary File-FigS21).



270

Figure S22 shows the time series correlations of the PMF factors' TS with external tracers for the period of W172303 (for expanded figure, see Supplementary File-FigS22).



275 **Figure S23 shows the time series correlations of the PMF factors' TS with external tracers for the period of M171115 (for expanded figure, see Supplementary File-FigS23).**

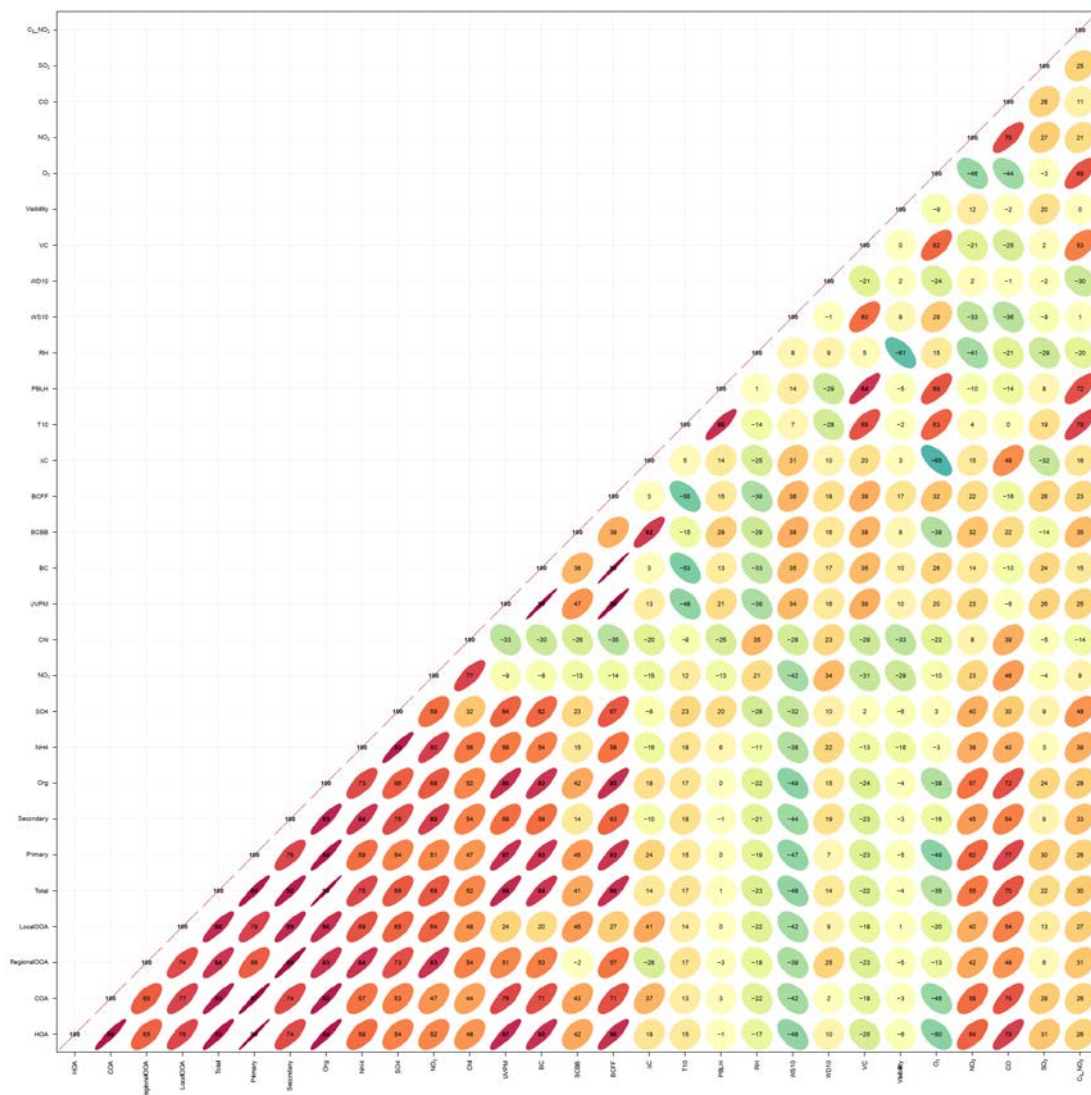


Figure S24 shows the time series correlations of the PMF factors' TS with external tracers for the period of M172303 (for expanded figure, see Supplementary File-FigS24).

S4 Details of time-of-day PMF oxidized organic aerosol MS and TS

280 S4.1 Time series patterns of secondary PM

In all time-of-day periods presented in the paper, POA and local OOA factors correlate more negatively with O₃ compared to the regional OOA factor, indicating O₃ co-production with regional OOA (Figs. S21–S24). Both midday and nighttime regional OOA factor TS correlate the strongest (among all PMF factors in their respective time periods) with O₃+NO₂, suggesting that daytime photochemistry and nighttime chemistry are the controlling processes for regional OOA production

285 respectively, with high primary emissions available for oxidation and higher OOA observed in periods with higher oxidant

levels. At midday in winter, one OOA factor shares similar time series correlations as the SFC-OA factor, suggesting similar origin (Fig. S21). This OOA factor has the highest correlations with sulfate in this period. We call this factor the local OOA factor, even though sulfate is generally associated with regional OOA. The other OOA factor at midday has low correlations with external tracers. At night, the local OOA factor correlates with nitrate and chloride, and the regional OOA factor correlates with sulfate and nitrate (Fig. S22). These differing correlations also suggest that the association of factors with inorganic species might be due to volatility and not similar origin, especially at midday in winter (Zhang et al., 2011). At monsoon midday, the regional OOA factor correlates strongly with sulfate and the local OOA factor correlates with nitrate (Fig. S23). Additionally, the monsoon midday local (and regional) OOA factor TS correlate strongly with O₃+NO₂, suggesting that rapid radical chemistry is the controlling process for OOA production. At monsoon nighttime, OOA factors are both correlated with sulfate and nitrate, but the OOA factor with weaker inorganic tracer correlations is correlated stronger with CO (Fig. S24). This factor also has lower MS correlations with the reference OOA profile (Fig. S26). We use these differences to attribute the local and regional OOA nature to the two factors at monsoon nighttime.

In all periods, time-of-day PMF OOA concentrations are within 25% of the seasonal PMF OOA concentrations, with lower concentrations in time-of-day PMF in all periods except winter nighttime (Figs. S31b and S32b). Unlike nighttime POA concentrations, nighttime OOA concentrations remain stable throughout. Also, unlike the large contrast in midday and nighttime POA concentrations, nighttime OOA concentrations are similar to midday OOA concentrations. The midday period is marked by higher atmospheric mixing, higher photochemical processing, and perhaps lower primary emissions than nighttime (Fig. S1). The nighttime periods are marked by inversions (Bhandari et al., 2020; Fig. S1). Together, these differences in meteorological variables and emissions likely lead to the stable nighttime OOA and similar midday and nighttime OOA concentrations.

S4.2 Mass spectral features of secondary factors

At winter midday, we observe higher contributions in time-of-day OOA at m/z 44, and lower contributions at m/z s 41 and 43, pointing to the higher oxidized nature of OOA (Fig. S33a). At monsoon midday, the only major difference is at m/z 43—higher contributions at m/z 43 lead to a lower oxidation state of OOA in time-of-day PMF (Fig. S34a). At nighttime in monsoon, we observe higher contributions at several m/z s \leq 44 in time-of-day PMF analysis, suggesting a higher oxidation of OOA (Fig. S34b). The similarity of the OOA MS comparisons in monsoon midday and winter nighttime is accompanied by a similarly strong correlation of the local OOA MS in these periods with the reference SVOOA MS (Figs. S25 and S26).

Here, we discuss in detail the comparison of lunch and nighttime OOA MS from the time-of-day PMF analysis and the seasonal PMF analysis (Sect. 3.4, Figs. S37–S38a–b). For both seasons, seasonal PMF analysis indicates more oxidized OOA at midday than nighttime, based on the higher contributions at m/z 44 (Zhang et al., 2011; Figs. S37a and S38a). In winter, this contrast is sharper in time-of-day PMF analysis and is in line with slower reaction chemistry at winter night (Fig. S37b). In monsoon, however, time-of-day PMF surprisingly suggests lesser oxidized OOA at midday than nighttime, with a higher contribution at m/z 43 and lower contribution at m/z 44 (Fig. S38b). The higher contributions of m/z 43 are likely caused

320 by the presence of semi-volatile compounds—monsoon midday local OOA profile shows the strongest correlation with the reference SVOOA MS among all OOA MS profiles presented in this paper (Fig. S26).

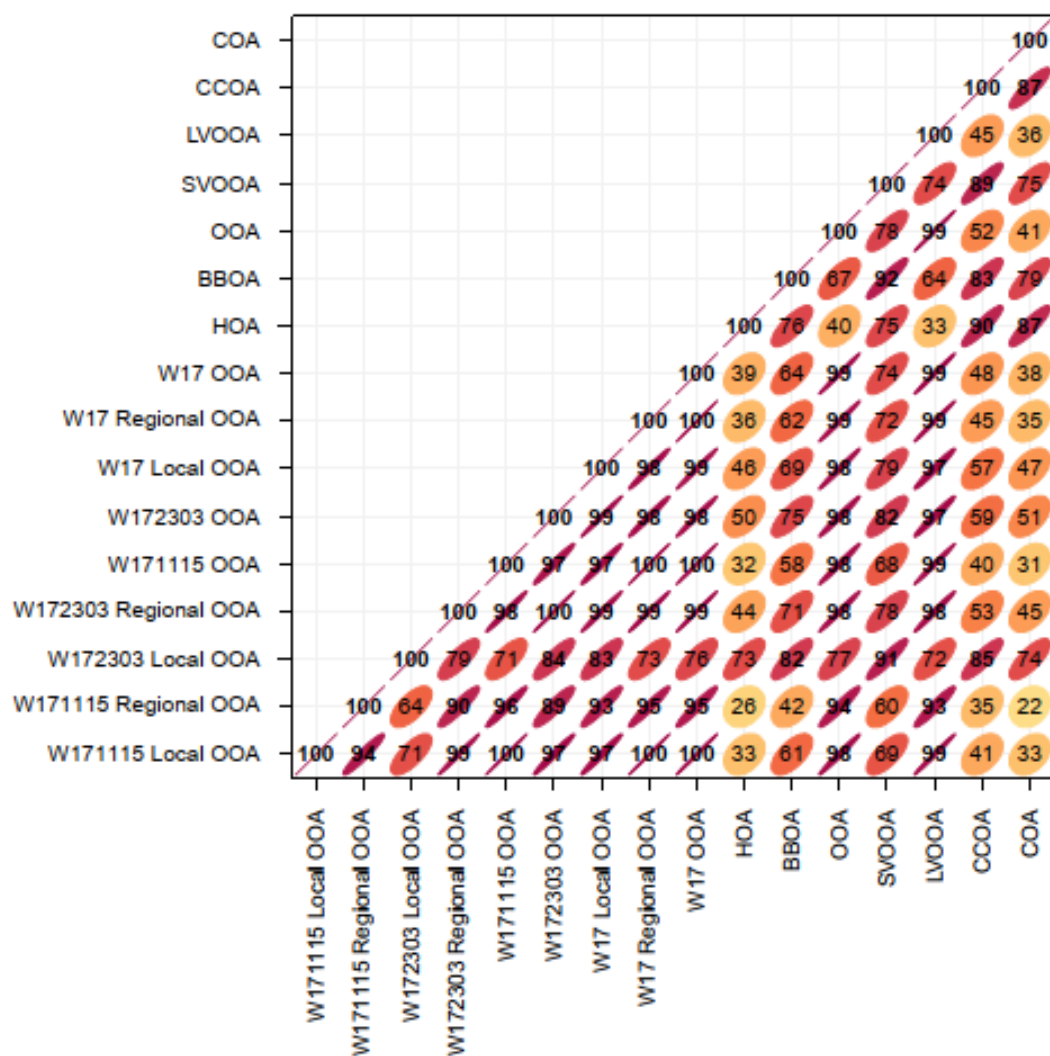
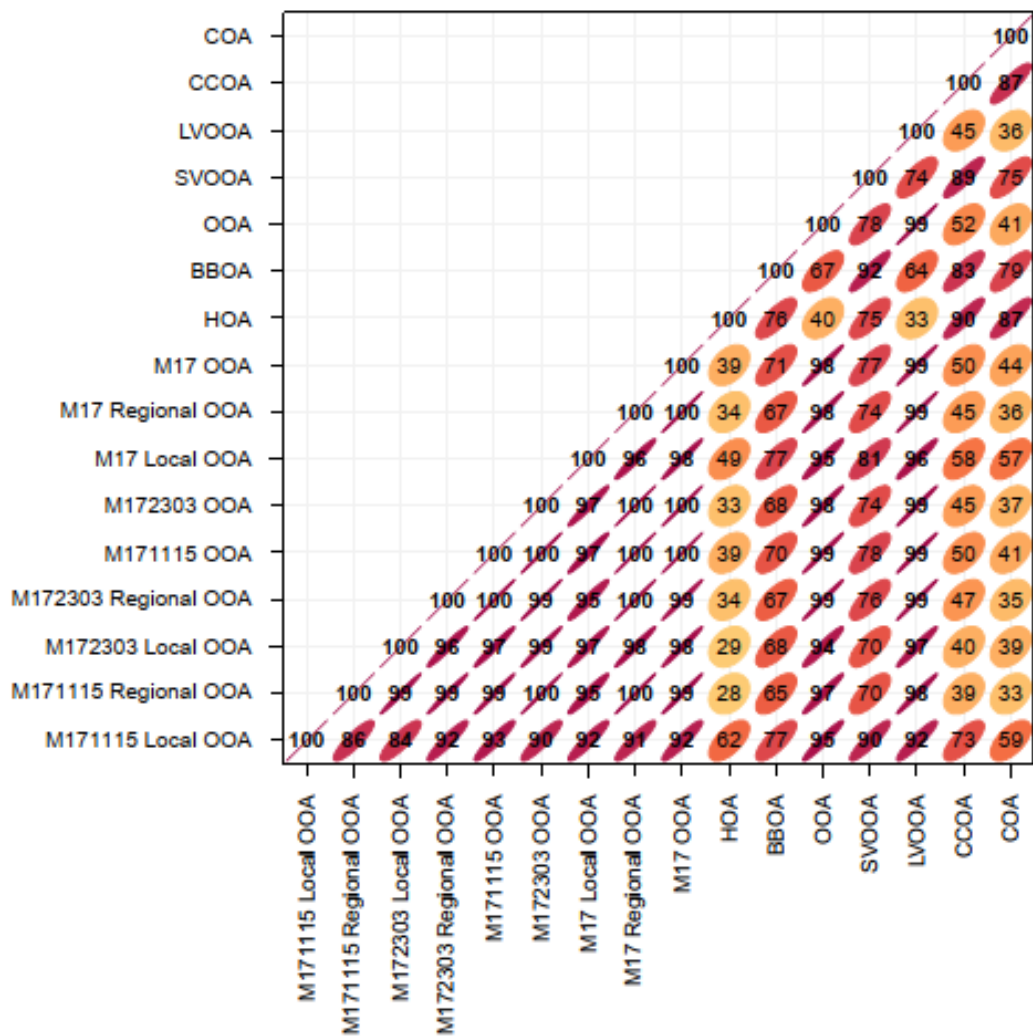


Figure S25 shows the time series correlations of the secondary PMF factors' MS with reference MS for the season of winter 2017. Regional OOA MS are more strongly correlated to reference OOA and LVOOA MS compared to local OOA MS. Local OOA MS are more strongly correlated to reference SVOOA MS compared to regional OOA.

325



330 Figure S26 shows the time series correlations of the secondary PMF factors' MS with reference MS for the season of monsoon 2017. Regional OOA MS are more strongly correlated to reference OOA and LVOOA MS compared to local OOA MS. Local OOA MS are more strongly correlated to reference SVOOA MS compared to regional OOA.

335

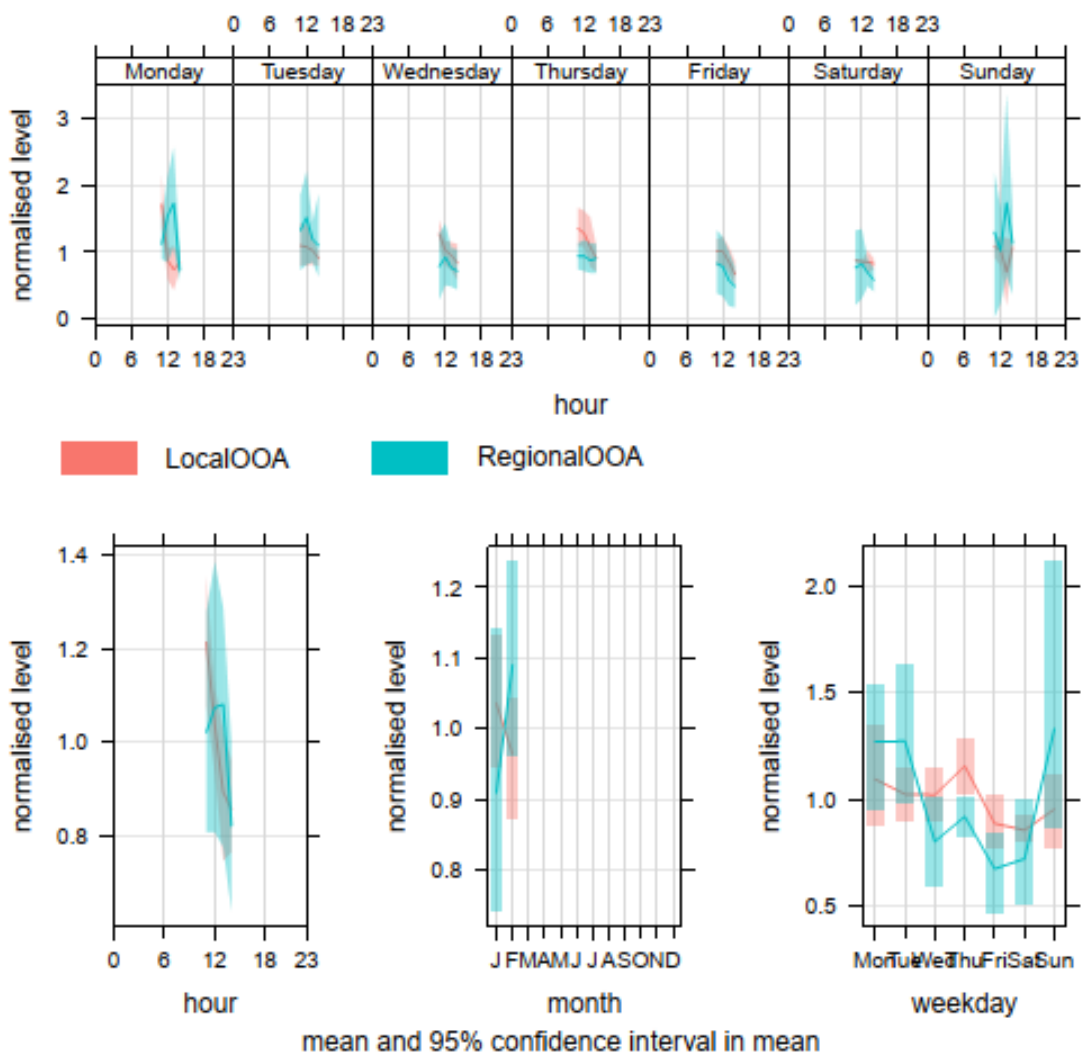
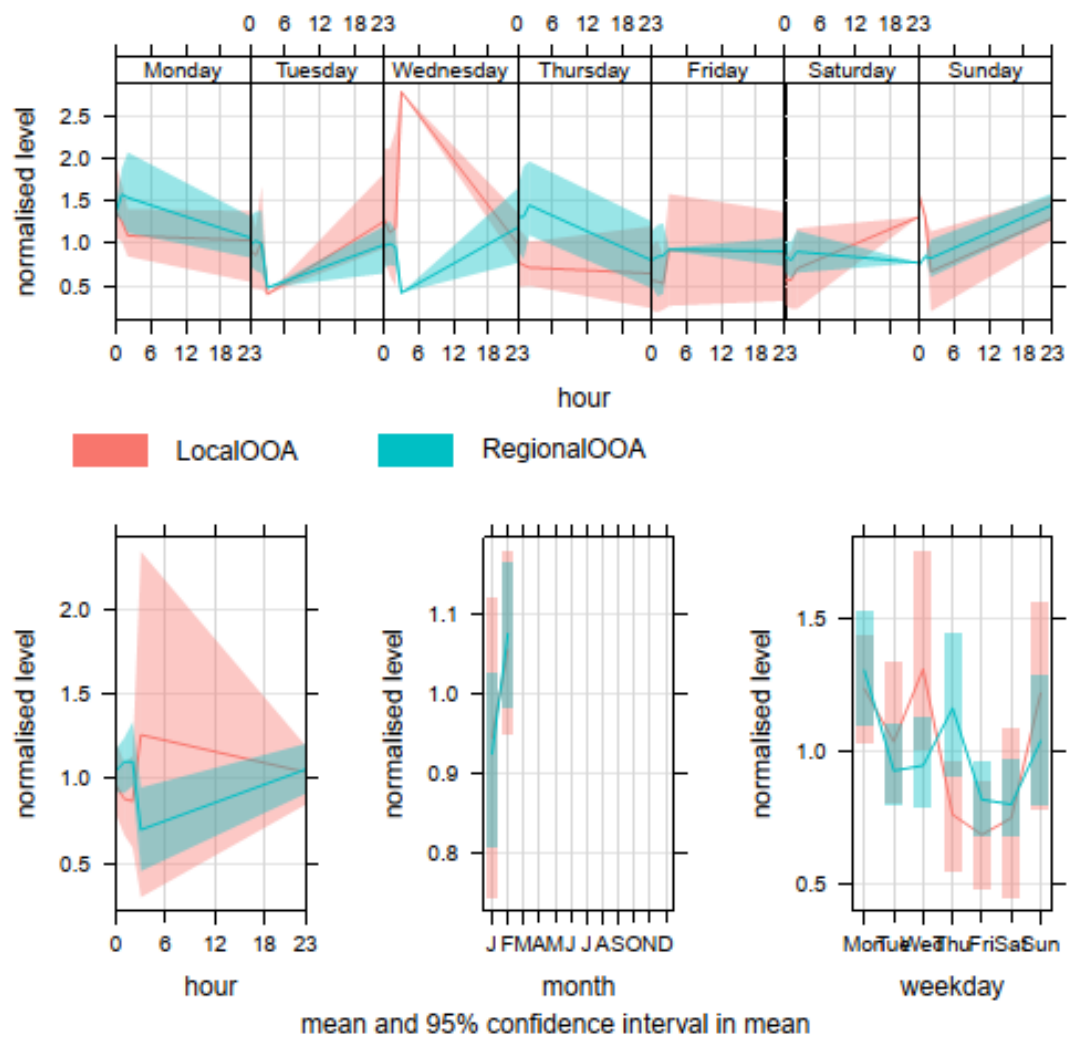
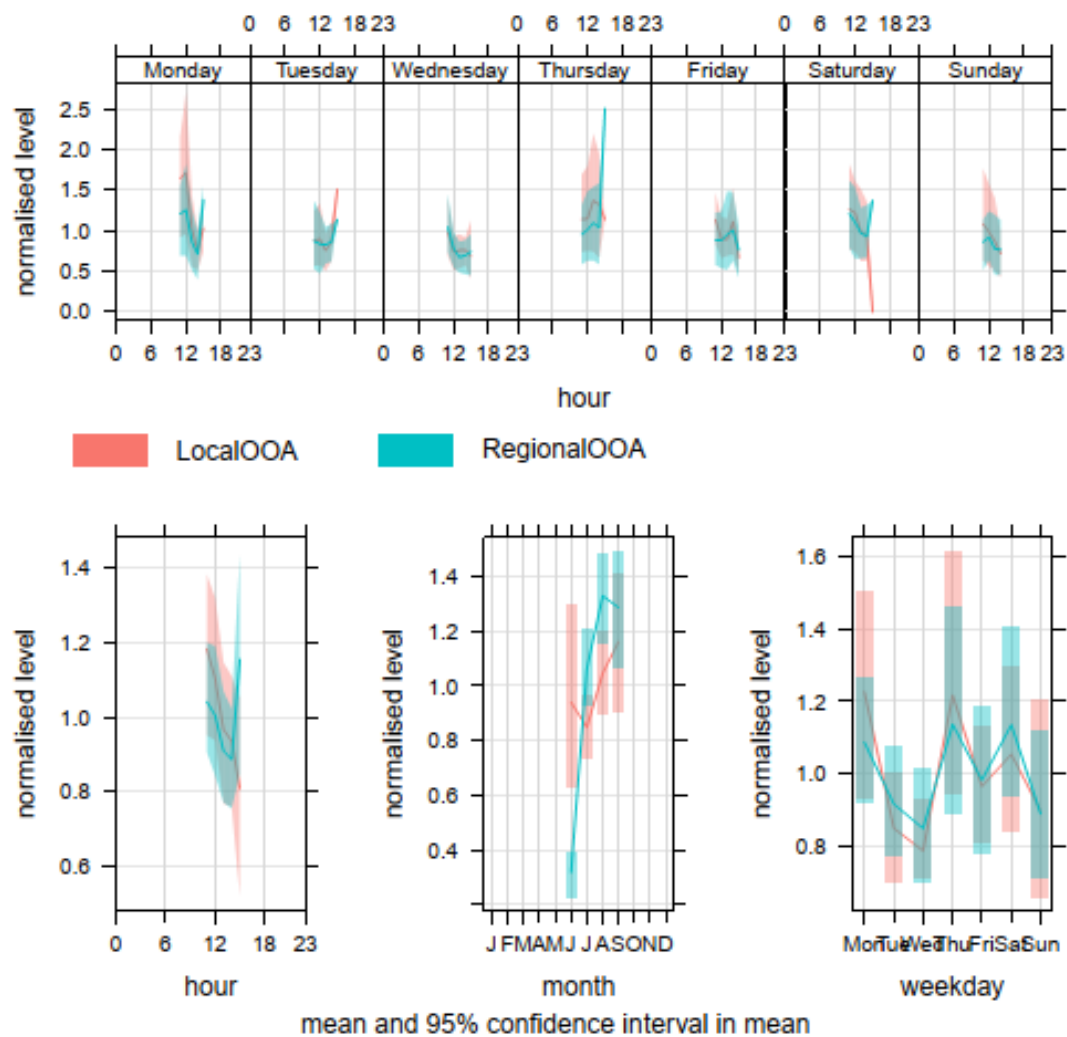


Figure S27 shows the hour-of-day on the day-of-week, seasonal diurnal, monthly, and week-of-day time series patterns for local OOA and regional OOA for the PMF run of W171115. Clearly, regional OOA is less variable diurnally than local OOA.



340 Figure S28 shows the hour-of-day on the day-of-week, seasonal diurnal, monthly, and week-of-day time series patterns for local OOA and regional OOA for the PMF run of W172303. Clearly, regional OOA is less variable diurnally than local OOA.



345 Figure S29 shows the hour-of-day on the day-of-week, seasonal diurnal, monthly, and week-of-day time series patterns for local OOA and regional OOA for the PMF run of M171115. Clearly, regional OOA is less variable diurnally than local OOA.

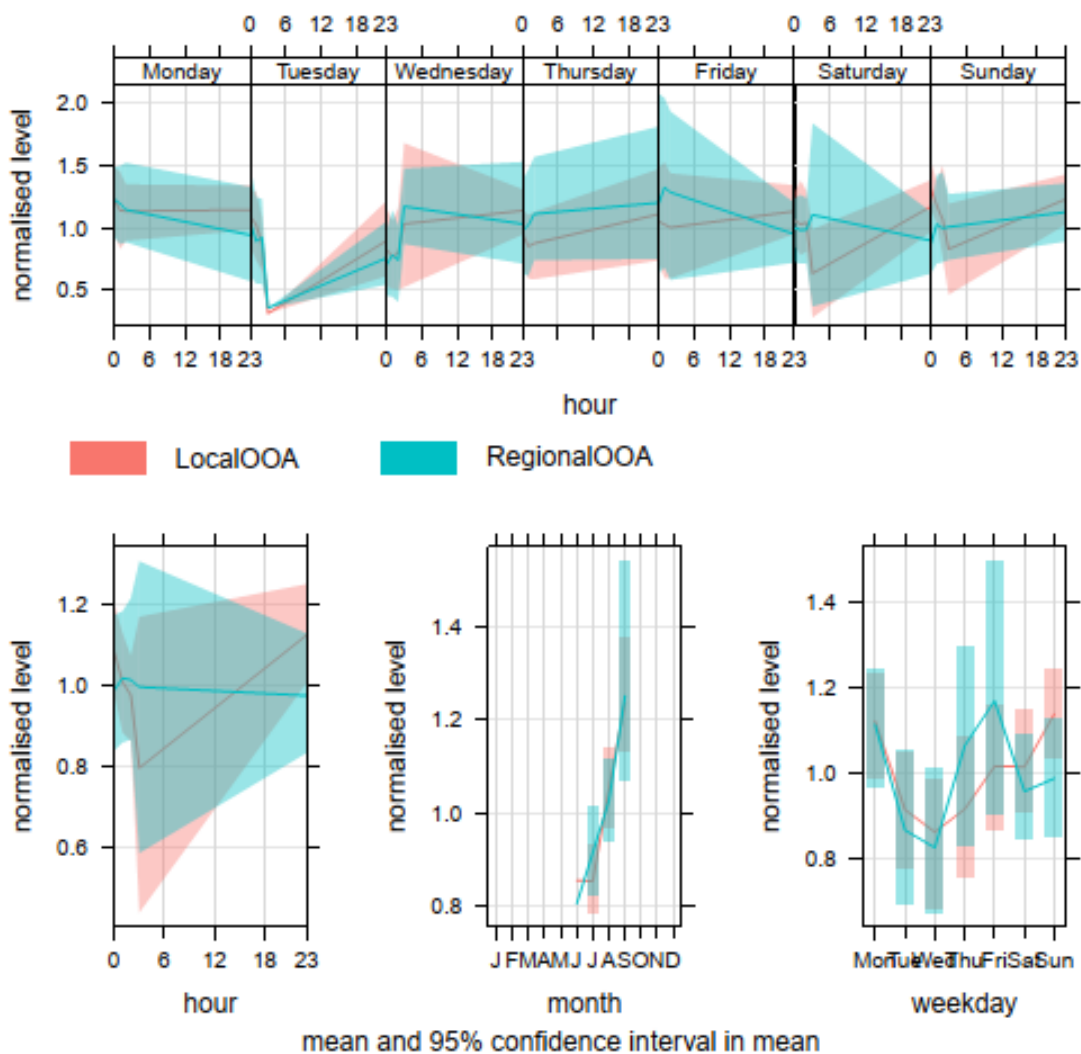


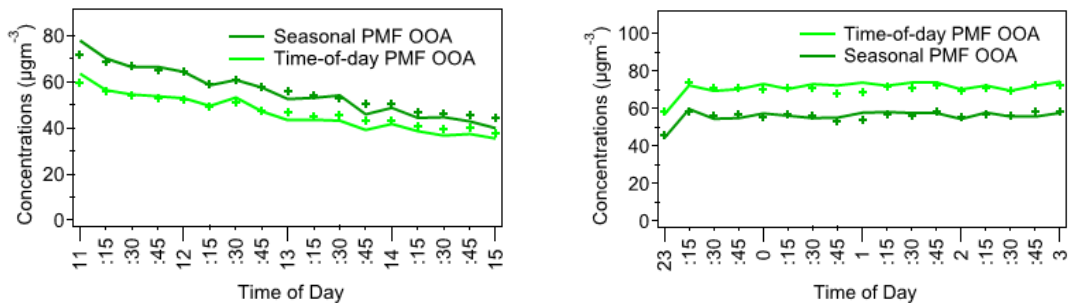
Figure S30 shows the hour-of-day on the day-of-week, seasonal diurnal, monthly, and week-of-day time series patterns for local OOA and regional OOA for the PMF run of M172303. Clearly, regional OOA is less variable diurnally than local OOA.

350

355

Table S11 Lowest and highest levels (relative to the normalization of 1) and the range (difference of the highest to the lowest levels) of local OOA and regional OOA (based on Figs. S27-S30)

Period	Lowest level		Highest level		Range (Highest – Lowest)	
	Local OOA	Regional OOA	Local OOA	Regional OOA	Local OOA	Regional OOA
W171115	0.86	0.82	1.21	1.08	0.35	0.26
W172303	0.87	0.71	1.26	1.11	0.39	0.40
M171115	0.81	0.89	1.18	1.15	0.37	0.26
M172303	0.79	0.97	1.12	1.02	0.33	0.05



365 **Figure S31** shows 15 min averaged concentration time series of OOA for the periods: (a) W171115 and (b) W172303.

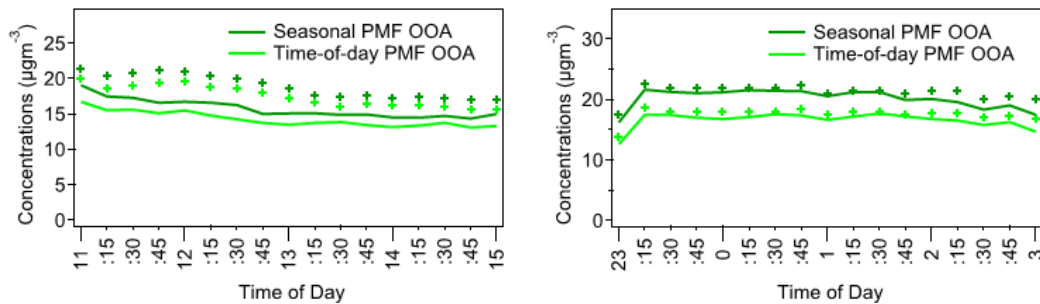
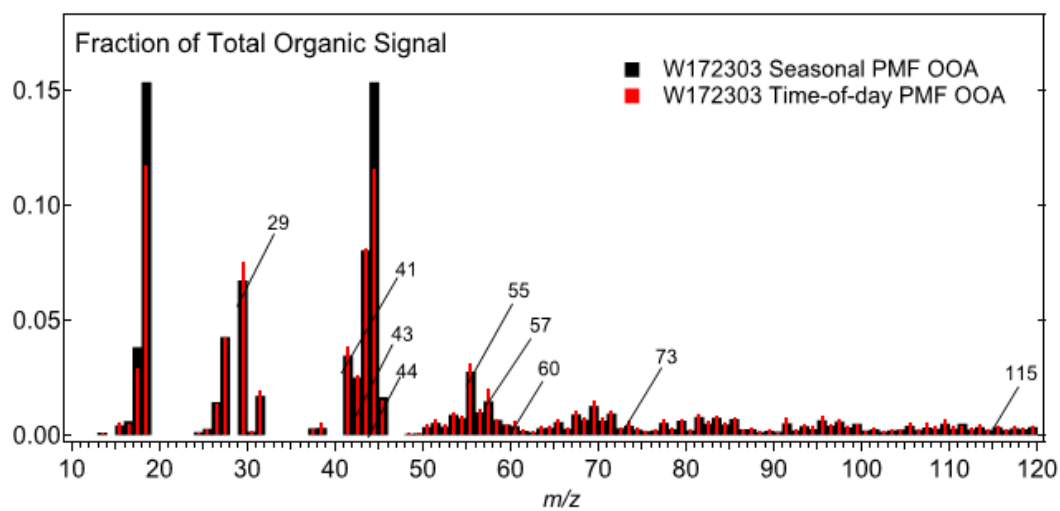
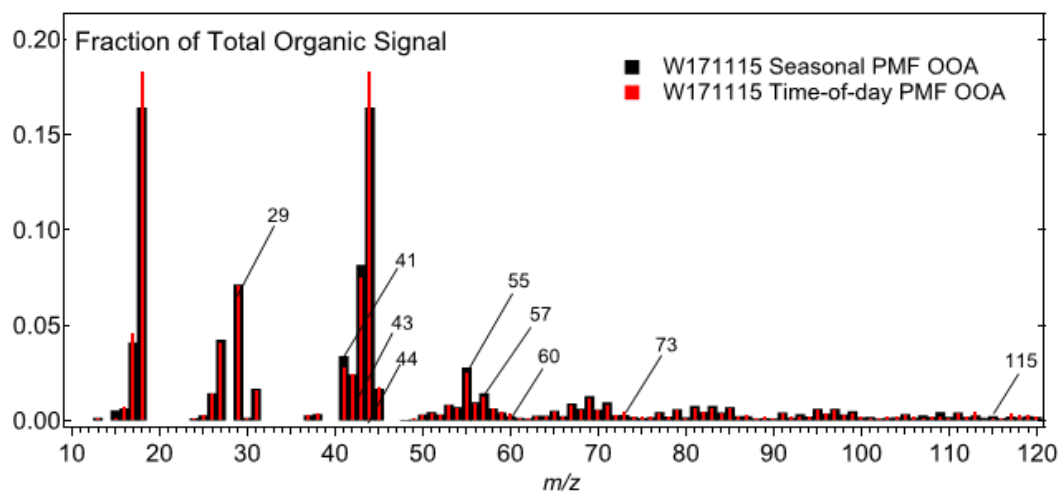
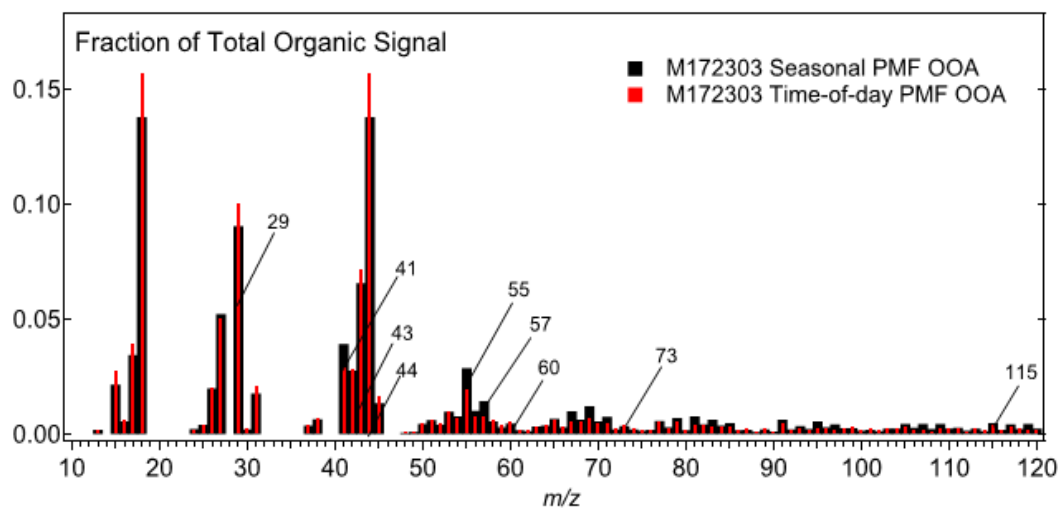
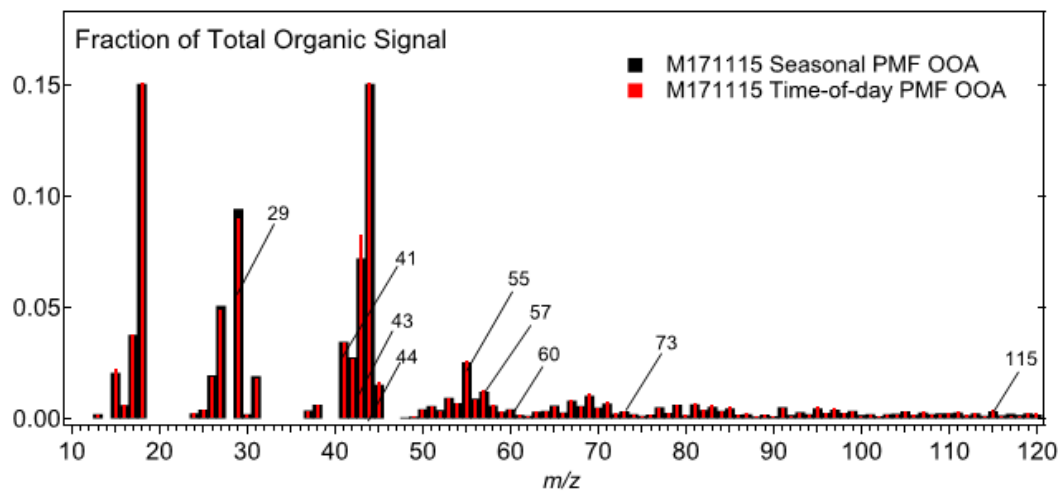


Figure S32 shows 15 min averaged concentration time series of OOA for the periods: (a) M171115 and (b) M172303.

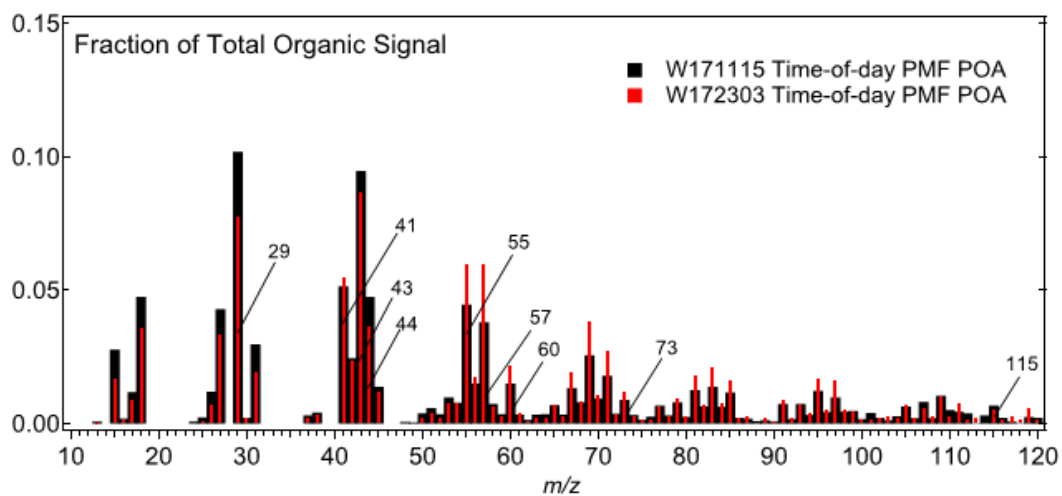
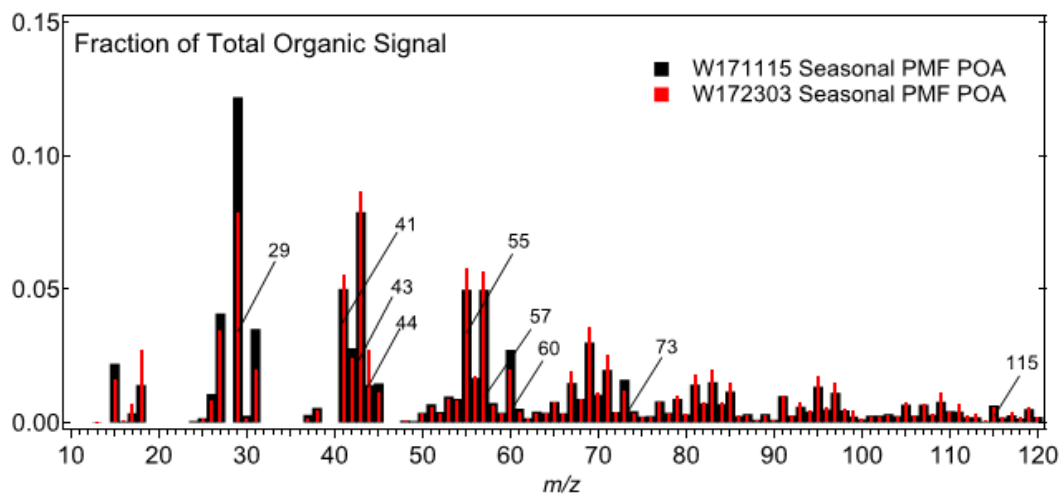


370

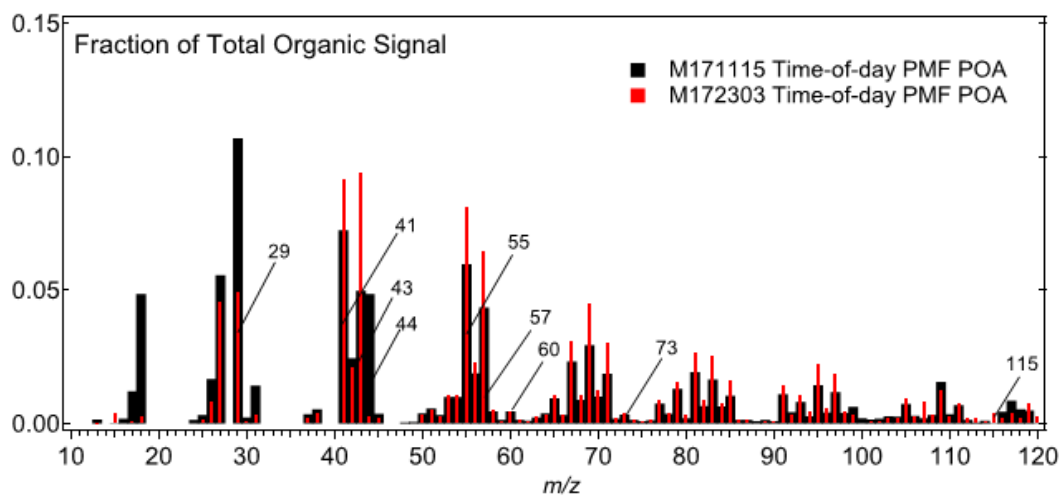
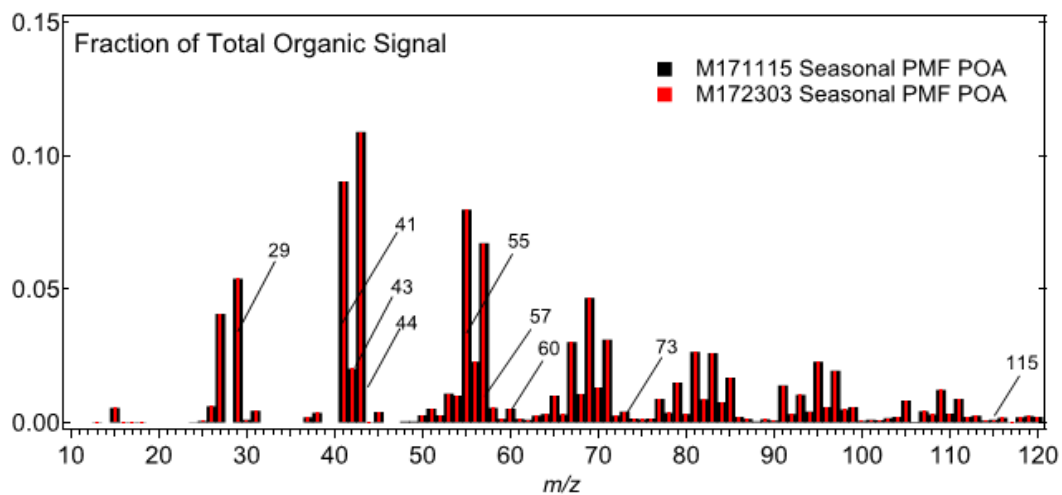
Figure S33 shows the mass spectra of (a) winter midday OOA, and (b) winter nighttime OOA using the seasonal PMF approach and the time-of-day PMF approach.



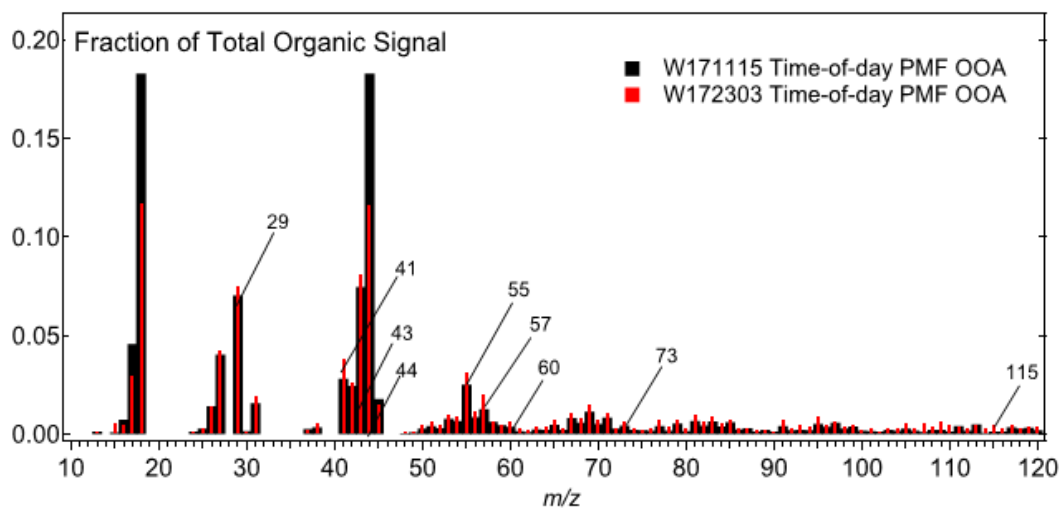
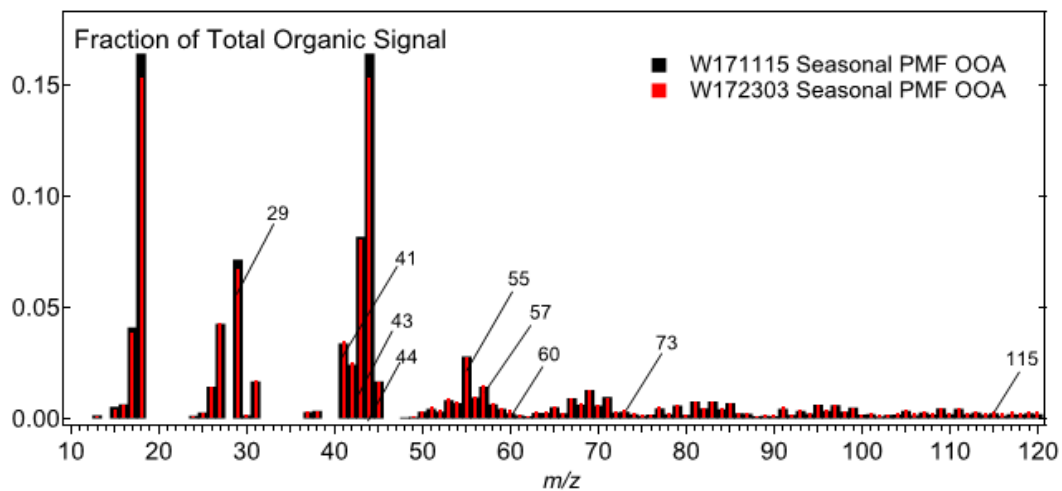
375 Figure S34 shows the mass spectra of (a) monsoon midday OOA, and (b) monsoon nighttime OOA using the seasonal PMF approach and the time-of-day PMF approach.



380 Figure S35 shows the mass spectra of winter midday and nighttime POA using (a) the seasonal PMF approach and (b) the time-of-day PMF approach. Both approaches indicate that the nighttime POA profiles show a stronger primary nature; however, the contrast is sharper in time-of-day PMF comparisons.



385 Figure S36 shows the mass spectra of monsoon midday and nighttime POA using (a) the seasonal PMF approach and (b) the time-of-day PMF approach. Only time-of-day PMF comparisons indicate that nighttime POA profiles show a stronger primary nature. Seasonal PMF comparisons show identical profiles.



390 **Figure S37 shows the mass spectra of winter midday and nighttime OOA using (a) the seasonal PMF approach and (b) the time-of-**
day PMF approach.

395

400

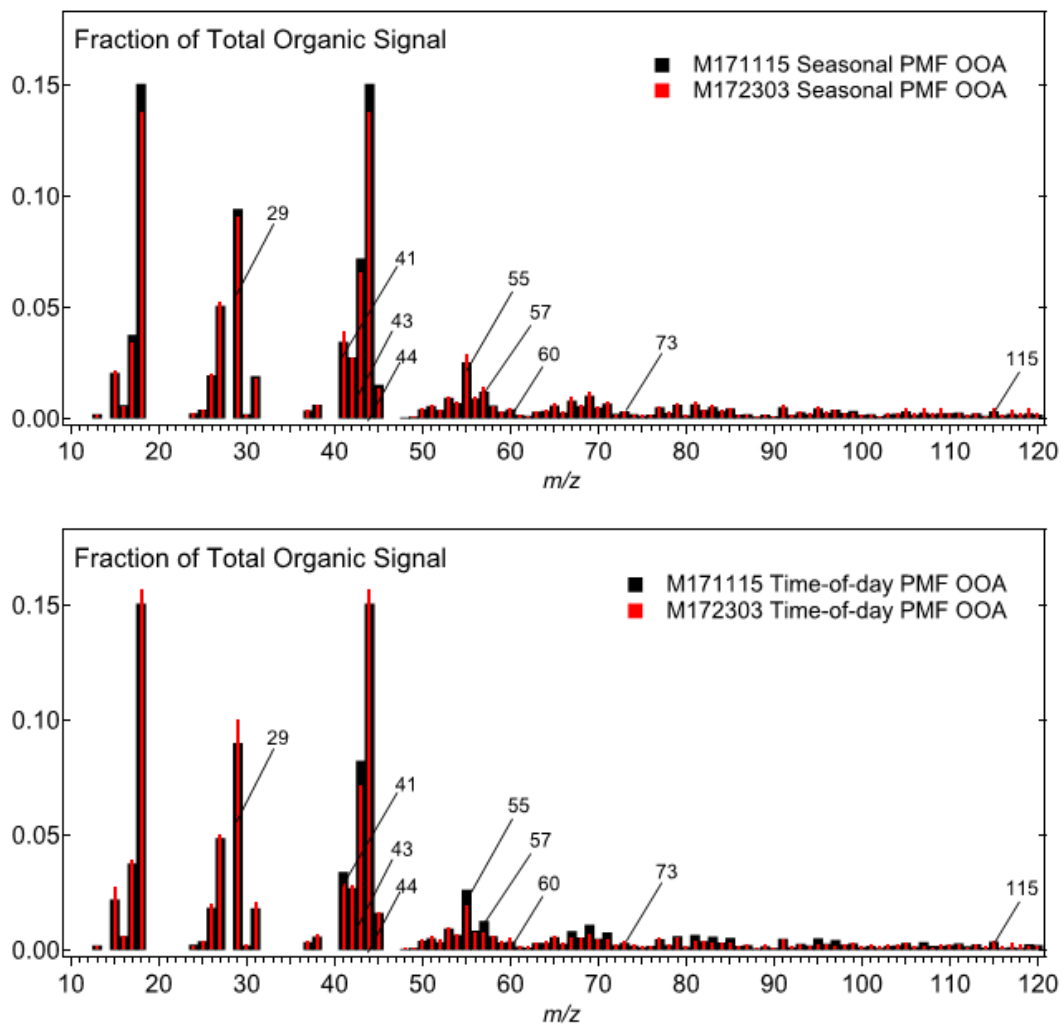
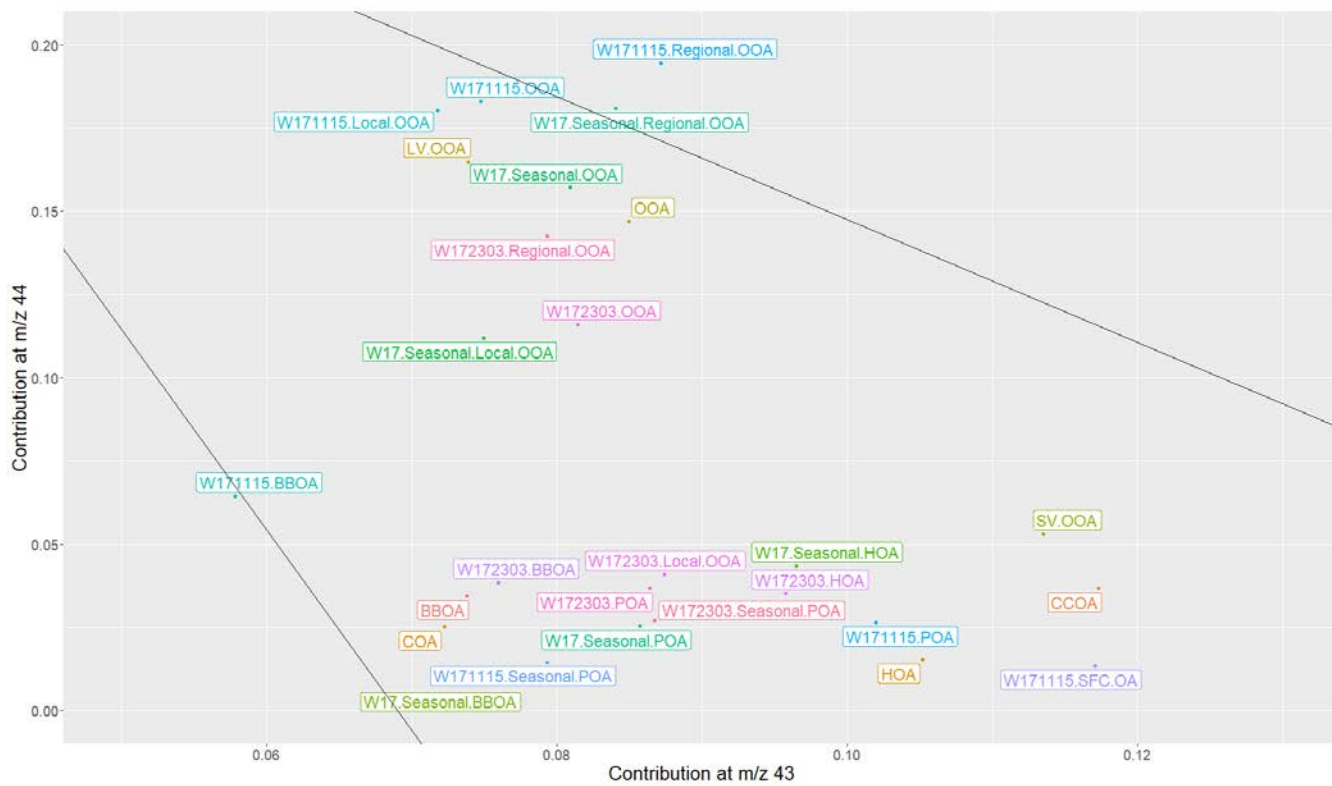


Figure S38 shows the mass spectra of monsoon midday and nighttime OOA using (a) the seasonal PMF approach and (b) the time-of-day PMF approach.



405 Figure S39 shows the obtained MS in this work plotted on the triangle plot (Ng et al., 2010)

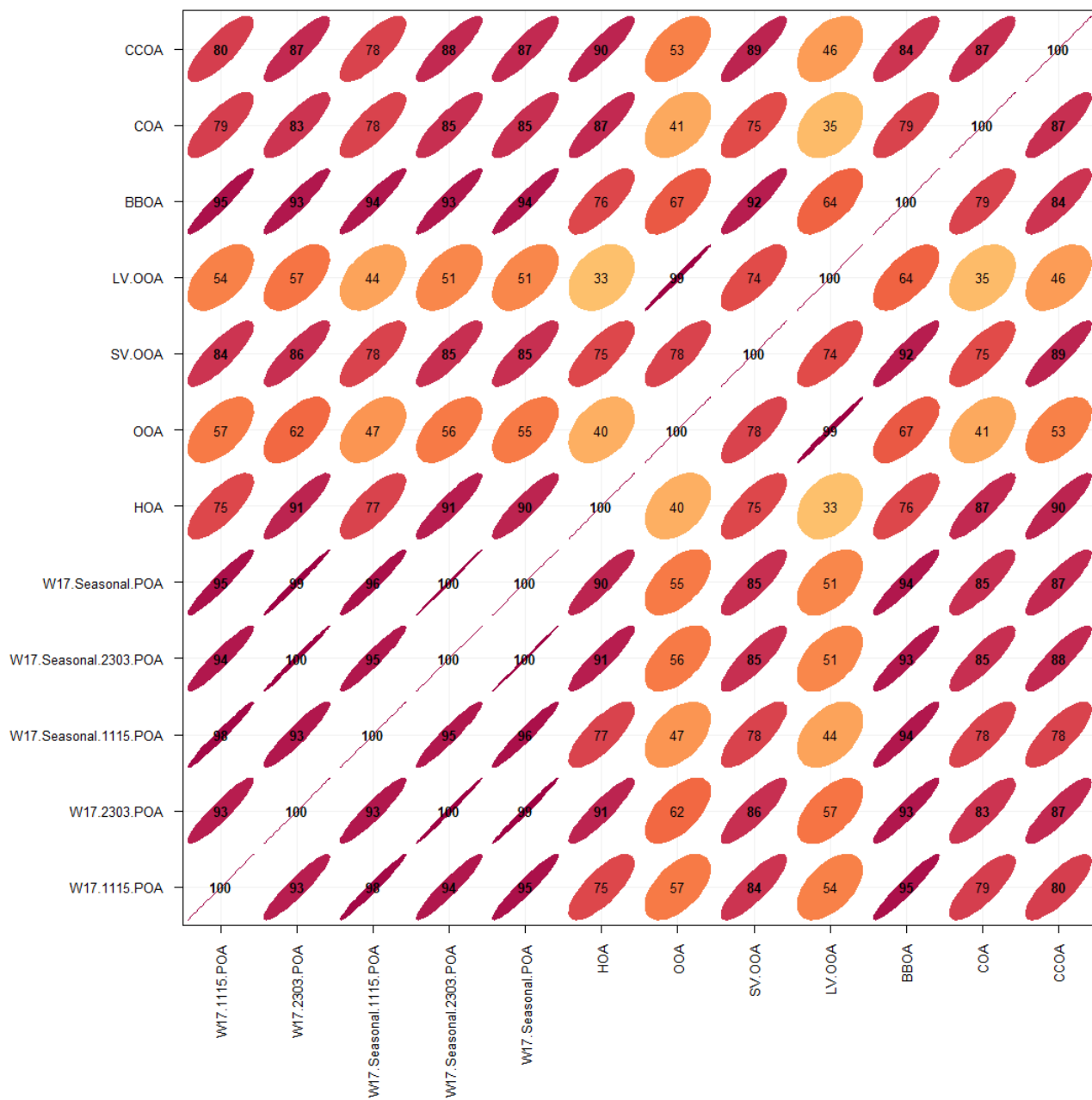


Figure S40 shows the mass spectral correlations of the primary PMF factors' MS with reference MS for the season of winter 2017. The time-of-day PMF midday and nighttime POA MS are less strongly correlated to each other than the seasonal PMF midday and nighttime POA MS.

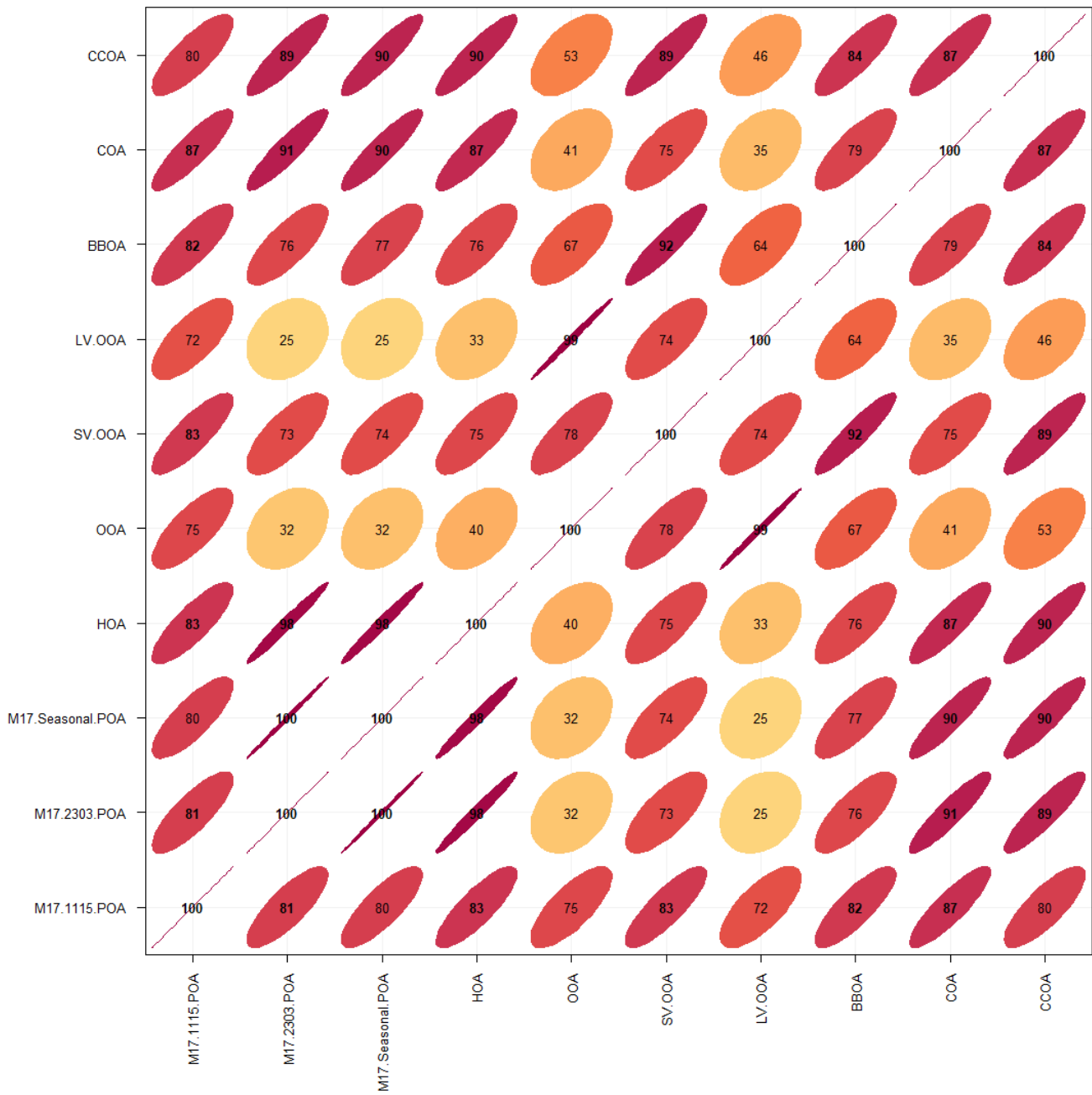
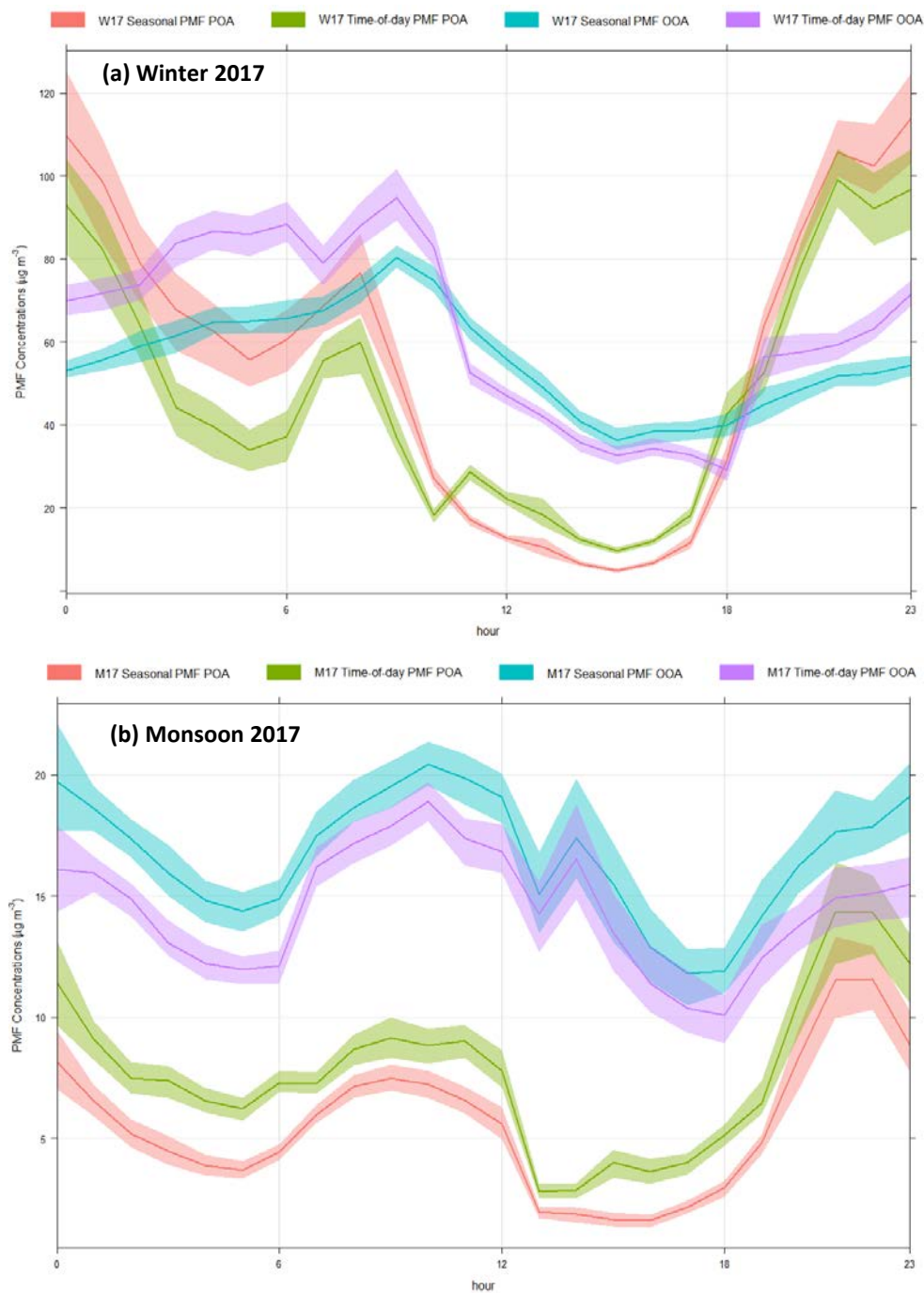


Figure S41 shows the time series correlations of the secondary PMF factors' MS with reference MS for the season of monsoon 2017. The time-of-day PMF midday and nighttime POA MS are less strongly correlated to each other than the seasonal PMF midday and nighttime POA MS.

415

S5 Summary of results from the companion paper



420 Figure S42a-b show the diurnal time series patterns of POA and OOA factors obtained from seasonal PMF and time-of-day PMF for winter and monsoon of 2017. The shaded areas represent the 95% confidence intervals.

Results from PMF analysis for all times of the day are presented in a companion paper (Bhandari et al., 2022). Here, we share a brief summary of those results, focusing on diurnal patterns of POA and OOA in seasonal PMF and time-of-day PMF. Figure 425 S41a-b show the diurnal time series patterns of POA (HOA+BBOA+COA) and OOA (Local OOA + Regional OOA) factors for winter and monsoon of 2017. Clearly, POA concentrations exhibit larger variability than OOA concentrations in both seasons. Our results show that the time series (TS) concentrations of time-of-day PMF factors are broadly consistent with seasonal PMF factors. In winter, we separated BBOA or BBOA-like factors in all periods but did not separate cooking organic aerosol (Table S3 in Bhandari et al., 2022). We also separated HOA or HOA-like factors in all time-of-day periods in winter. 430 In monsoon 2017, we separated HOA or HOA-like factors, and COA or COA-like factors in all time-of-day periods but did not separate biomass burning organic aerosol above detection limits (Tables 2, S3 in Bhandari et al., 2022). The behaviour of POA and OOA TS obtained by combining all time-of-day PMF results suggests strong similarities to seasonal PMF POA and OOA TS, respectively (W17 POA: slope ~ 0.83 , intercept ~ 1.6 , $R \sim 0.97$; W17 OOA: slope ~ 1.26 , intercept ~ -7.0 , $R \sim 0.88$; M17 POA: slope ~ 1.15 , intercept ~ 1.5 , $R \sim 0.97$; M17 OOA: slope ~ 0.91 , intercept ~ -0.5 , $R \sim 0.98$). In winter, we observe 435 largest differences in POA TS diurnal concentrations midday where primary concentrations are higher in time-of-day PMF by $\geq 40\%$. Because of the low total OA concentrations in these periods, they likely have limited importance in seasonal PMF analysis with respect to determining the overall seasonal mass spectra and time series patterns, and thus conducting time-of-day PMF analysis results in factors exhibiting substantial deviations from seasonal analysis. In monsoon, seasonal PMF analysis underestimates POA concentrations throughout the day. Finally, we also observe that winter time-of-day PMF OOA 440 time series patterns exhibit significantly lower diurnal variability than time-of-day PMF POA but stronger diurnal variability than seasonal PMF OOA. For the time-of-day PMF approach, winter peak OOA diurnal concentrations in the morning (0900–1000 hours) are ~ 2.7 times the diurnal minimum (which occurs in the evening, 1800–1900 hours); substantially greater than the ~ 2.2 observed for seasonal PMF winter OOA concentrations. This difference is driven by lower OOA concentrations midday (1100–1900 hours) and higher OOA concentrations at other hours. In monsoon, OOA concentrations show similar 445 diurnal patterns between time-of-day PMF and seasonal PMF and OOA concentrations are almost always lower in time-of-day PMF. Clearly, time-of-day PMF captures different aspects of diurnal variability better than seasonal PMF, and which is a major advantage of this new approach.

450 S6 References

1. Bhandari, S., Gani, S., Patel, K., Wang, D. S., Soni, P., Arub, Z., Habib, G., Apte, J. S., and Ruiz, L. H.: Sources and atmospheric dynamics of organic aerosol in New Delhi, India: insights from receptor modeling, *Atmospheric Chemistry and Physics*, 20, 735–752, URL <https://acp.copernicus.org/articles/20/735/2020/>, 2020.
2. Canonaco, F., Slowik, J. G., Baltensperger, U., and Prévôt, A. S. H.: Seasonal differences in oxygenated organic
455 aerosol composition: implications for emissions sources and factor analysis, *Atmospheric Chemistry and Physics*, 15, 6993–7002, URL <https://acp.copernicus.org/articles/15/6993/2015/>, 2015.
3. Carslaw, D. C. and Ropkins, K.: openair: an R package for air quality data analysis, *Environmental Modelling and Software*, 27–28, 52–61, URL <https://doi.org/10.1016/j.envsoft.2011.09.008>, 2012.
4. Crippa, M., Solazzo, E., Huang, G., Guizzardi, D., Koffi, E., Muntean, M., Schieberle, C., Friedrich, R., and
460 Janssens-Maenhout, G.: High resolution temporal profiles in the Emissions Database for Global Atmospheric Research, *Scientific Data*, 7, 1–17, URL <https://www.nature.com/articles/s41597-020-0462-2>, 2020.
5. Fröhlich, R., Crenn, V., Setyan, A., Belis, C. A., Canonaco, F., Favez, O., Riffault, V., Slowik, J. G., Aas, W., Aijälä, M., Alastuey, A., Artiñano, S., Bonnaire, N., Bozzetti, C., Bressi, M., Carbone, C., Coz, E., Croteau, P. L., Cubison, M. J., Esser-Gietl, J. K., Green, D. C., Gros, V., Heikkinen, L., Herrmann, H., Jayne, J. T., Lunder, C. R., Minguillón, M. C., Mocnik, G., O’Dowd, C. D., Ovadnevaite, J., Petralia, E., Poulain, L., Priestman, M., Ripoll, A., Sarda-Estève, R., Wiedensohler, A., Baltensperger, U., Sciare, J., and Prévôt, A. S. H.: ACTRIS ACSM intercomparison–Part 2: intercomparison of ME-2 organic source apportionment results from 15 individual, co-located aerosol mass spectrometers, *Atmospheric Measurement Techniques*, 8, 2555–2576, URL <https://amt.copernicus.org/articles/8/2555/2015/>, 2015.
- 470 6. Gani, S., Bhandari, S., Seraj, S., Wang, D. S., Patel, K., Soni, P., Arub, Z., Habib, G., Hildebrandt Ruiz, L., and Apte, J.: Submicron aerosol composition in the world’s most polluted megacity: The Delhi Aerosol Supersite study, *Atmos. Chem. Phys.*, 19, 6843–6859, URL <https://doi.org/10.5194/acp-19-6843-2019>, 2019.
7. Grolemond, G. and Wickham, H.: Dates and times made easy with lubridate, *Journal of Statistical Software*, 40, 1–25, URL <http://www.jstatsoft.org/v40/i03/>, 2011.
- 475 8. Hayfield, T. and Racine, J. S.: Nonparametric econometrics: the np package, *Journal of Statistical Software*, 27, URL <http://www.jstatsoft.org/v27/i05/>, 2008.
9. Hemann, J. G., Brinkman, G. L., Dutton, S. J., Hannigan, M. P., Milford, J. S., and Miller, S.L.: Assessing positive matrix factorization model fit: a new method to estimate uncertainty and bias in factor contributions at the measurement time scale, *Atmospheric Chemistry and Physics*, 9, 497–513, URL <https://acp.copernicus.org/articles/9/497/2009/>, 2009.
- 480

10. Jimenez, J. L., Canagaratna, M. R., Donahue, N. M., Prevot, A. S., Zhang, Q., Kroll, J. H., DeCarlo, P. F., Allan, J. D., Coe, H., Ng, N. L., Aiken, A. C., Docherty, K. S., Ulbrich, I. M., Grieshop, A. P., Robinson, A. L., Duplissy, J., Smith, J. D., Wilson, K. R., Lanz, V. A., Hueglin, C., Sun, Y. L., Tian, J., Laaksonen, A., Raatikainen, T., Rautiainen, J., Vaattovaara, P., Ehn, M., Kulmala, M., Tomlinson, J. M., Collins, D. R., Cubison, M. J., Dunlea, E. J., Huffman, J. A., Onasch, T. S., Alfarra, M. R., Williams, P. I., Bower, K., Kondo, Y., Schneider, J., Drewnick, F., Borrmann, S., Weimer, S., Demerjian, K., Salcedo, D., Cottrell, L., Griffin, R., Takami, A., Miyoshi, T., Hatakeyama, S., Shimojo, A., Sun, J. Y., Zhang, Y. M., Dzepina, K., Kimmel, J. R., Sueper, D., Jayne, J. T., Herndon, S. C., Trimborn, A. M., Williams, L. R., Wood, E. C., Middlebrook, A. M., Kolb, C. E., Baltensperger, U., and Worsnop, D. R.: Evolution of organic aerosols in the atmosphere, *Science*, 326, 1525–1529, URL <https://science.sciencemag.org/content/326/5959/1525>, 2009.
11. Ng, N. L.; Canagaratna, M. R.; Zhang, Q.; Jimenez, J. L.; Tian, J.; Ulbrich, I. M.; Kroll, J. H.; Docherty, K. S.; Chhabra, P. S.; Bahreini, R.; Murphy, S. M.; Seinfeld, J. H.; Hildebrandt, L.; Donahue, N. M.; DeCarlo, P. F.; Lanz, V. A.; Prévôt, A. S. H.; Dinar, E.; Rudich, Y.; Worsnop, D. R. Organic Aerosol Components Observed in Northern Hemispheric Datasets from Aerosol Mass Spectrometry. *Atmospheric Chemistry and Physics*, 10 (10), 4625–4641. URL <https://doi.org/10.5194/acp-10-4625-2010>, 2010.
12. Ng, N. L., Herndon, S. C., Trimborn, A., Canagaratna, M. R., Croteau, P. L., Onasch, T. S., Sueper, D., Worsnop, D. R., Zhang, Q., Sun, Y. L., and Jayne, J. T.: An Aerosol Chemical Speciation Monitor (ACSM) for routine monitoring of the composition and mass concentrations of ambient aerosol, *Aerosol Science and Technology*, 45, 780–794, URL <http://www.tandfonline.com/doi/abs/10.1080/02786826.2011.560211>, 2011.
13. Norris, G., Duvall, R., Brown, S., and Bai, S.: EPA Positive Matrix Factorization 5.0 fundamentals and user guide, URL <https://www.epa.gov/air-research/epa-positive-matrix-factorization-50-fundamentals-and-user-guide>, 2014.
14. Olson, M. R., Garcia, M. V., Robinson, M. A., Rooy, P. V., Dietenberger, M. A., Bergin, M., and Schauer, J. J.: Investigation of black and brown carbon multiple-wavelength dependent light absorption from biomass and fossil fuel combustion source emissions, *Journal of Geophysical Research*, 120, 6682–6697, URL <https://doi.org/10.1002/2014JD022970>, 2015.
15. Paatero, P. and Hopke, P. K.: Discarding or downweighting high-noise variables in factor analytic models, *Analytica Chimica Acta*, 490, 277–289, URL [https://doi.org/10.1016/S0003-2670\(02\)01643-4](https://doi.org/10.1016/S0003-2670(02)01643-4), 2003.
16. Paatero, P. and Hopke, P. K.: Rotational tools for factor analytic models, *Journal of Chemometrics*, 23, 91–100, URL <http://doi.wiley.com/10.1002/cem.1197>, 2009.
17. Paatero, P., Eberly, S., Brown, S. G., and Norris, G. A.: Methods for estimating uncertainty in factor analytic solutions, *Atmospheric Measurement Techniques*, 7, 781–797, URL <https://amt.copernicus.org/articles/7/781/2014/>, 2014.
18. Politis, D. N. and White, H.: Automatic block-length selection for the dependent bootstrap, *Econometric Reviews*, 23, 53–70, URL <https://www.tandfonline.com/doi/abs/10.1081/ETC-120028836>, 2004.

- 515 19. Patton, A., Politis, D. N., and White, H.: Correction to automatic block-length selection for the dependent bootstrap by D. Politis and H. White, *Econometric Reviews*, 28, 372–375, URL <https://doi.org/10.1080/07474930802459016>, 2009.
20. R Core Team: R: a language and environment for statistical computing, R Foundation for Statistical Computing, Vienna, Austria, URL <https://www.R-project.org/>, 2019.
- 520 21. ResearchGate, <https://www.researchgate.net/post/Has-anybody-observed-strange-discontinuities-in-ERA5s-diurnal-cycle-of-temperature-precipitation-etc>, 2021.
22. Sandradewi, J., Prévôt, A. S., Szidat, S., Perron, N., Alfarra, M. R., Lanz, V. A., Weingartner, E., and Baltensperger, U. R.: Using aerosol light absorption measurements for the quantitative determination of wood burning and traffic emission contribution to particulate matter, *Environmental Science and Technology*, 42, 3316–3323, URL <https://doi.org/10.1021/es702253m>, 2008.
- 525 23. Schlag, P., Kiendler-Scharr, A., Blom, M. J., Canonaco, F., Henzing, J. S., Moerman, M., Prévôt, A. S. H., and Holzinger, R.: Aerosol source apportionment from 1-year measurements at the CESAR tower in Cabauw, the Netherlands, *Atmospheric Chemistry and Physics*, 16, 8831–8847, URL <https://acp.copernicus.org/articles/16/8831/2016/>, 2016.
- 530 24. Tian, J., Wang, Q., Ni, H., Wang, M., Zhou, Y., Han, Y., Shen, Z., Pongpiachan, S., Zhang, N., Zhao, Z., Zhang, Q., Zhang, Y., Long, X., and Cao, J.: Emission characteristics of primary brown carbon absorption from biomass and coal burning: development of an optical emission inventory for China, *Journal of Geophysical Research: Atmospheres*, 124, URL <https://onlinelibrary.wiley.com/doi/abs/10.1029/2018JD029352>, 2019.
- 535 25. Tobler, A., Bhattu, D., Canonaco, F., Lalchandani, V., Shukla, A., Thamban, N. M., Mishra, S., Srivastava, A. K., Bisht, D. S., Tiwari, S., Singh, S., Mocnik, G., Baltensperger, U., Tripathi, S. N., Slowik, J. G., and Prévôt, A. S.: Chemical characterization of PM_{2.5} and source apportionment of organic aerosol in New Delhi, India, *Science of the Total Environment*, 745, URL <https://doi.org/10.1016/j.scitotenv.2020.140924>, 2020.
- 540 26. Ulbrich, I. M., Canagaratna, M. R., Zhang, Q., Worsnop, D. R., and Jimenez, J. L.: Interpretation of organic components from positive matrix factorization of aerosol mass spectrometric data, *Atmos. Chem. Phys.*, 9, 2891–2918, URL <https://doi.org/10.5194/acp-9-2891-2009>, 2009.
27. Ulbrich, I. M., Handschy, A., Lechner, M., and Jimenez, J.: AMS Spectral Database, URL <http://cires.colorado.edu/jimenez-group/AMSsd/> (last access: 25 April 2019), 2017.
28. Ulbrich, I. M., Handschy, A., Lechner, M., and Jimenez, J.: High-Resolution AMS Spectral Database, URL <http://cires.colorado.edu/jimenez-group/HRAMSsd/> (last access: 25 April 2019), 2018.
- 545 29. Venables, W. N. and Ripley, S. D.: *Modern applied statistics with S*, Springer, New York, fourth edn., URL <http://www.stats.ox.ac.uk/pub/MASS4>, 2002.

30. Wang, Y., Hopke, P. K., Rattigan, O. V., Xia, X., Chalupa, D. C., and Utell, M. J.: Characterization of residential wood combustion particles using the two-wavelength aethalometer, *Environmental Science and Technology*, 45, 7387–7393, URL <https://doi.org/10.1021/es2013984>, 2011.
- 550 31. Wickham, H., Averick, M., Bryan, J., Chang, W., McGowan, L. D., François, R., Grolemund, G., Hayes, A., Henry, L., Hester, J., Kuhn, M., Pedersen, T. L., Miller, E., Bache, S. M., Müller, K., Ooms, J., Robinson, D., Seidel, D. P., Spinu, V., Takahashi, K., Vaughan, D., Wilke, C., Woo, K., and Yutani, H.: Welcome to the tidyverse, *Journal of Open Source Software*, 4, URL <https://joss.theoj.org/papers/10.21105/joss.01686>, 2019.
- 555 32. Zhang, Q., Jimenez, J. L., Canagaratna, M. R., Ulbrich, I. M., Ng, N. L., Worsnop, D. R., and Sun, Y.: Understanding atmospheric organic aerosols via factor analysis of aerosol mass spectrometry: a review, *Analytical and Bioanalytical Chemistry*, 401, 3045–3067, URL <https://link.springer.com/article/10.1007/s00216-011-5355-y>, 2011.
- 560 33. Zhu, Q., Huang, X.-F., Cao, L.-M., Wei, L.-T., Zhang, S, He, L.-Y., Elser, M., Canonaco, F., Slowik, J. G., Bozzetti, C., El-Haddad, I., and Prévôt, A. S. H.: Improved source apportionment of organic aerosols in complex urban air pollution using the multilinear engine (ME-2), *Atmospheric Measurement Techniques*, 11, 1049–1060, URL <https://amt.copernicus.org/articles/11/1049/2018/>, 2018.